Calcium binding at the C-terminus of α-synuclein modulates synaptic vesicle interaction

Janin Lautenschläger[1#], Amberley D. Stephens[1#], Giuliana Fusco[2,3], Florian Ströhl[1], Nathan Curry[1], Maria Zacharopoulou[1], Claire H. Michel[1], Romain Laine[1], Nadezhda Nespovitaya[1], Marcus Fantham[1], Dorothea Pinotsi[1,4], Wagner Zago[5], Paul Fraser[6], Anurag Tandon[6], Peter St George-Hyslop[6,7], Eric Rees[1], Jonathan J. Phillips[8], Alfonso De Simone[3], Clemens F. Kaminski[1], Gabriele S. Kaminski Schierle[1]*

[1]Department of Chemical Engineering and Biotechnology, University of Cambridge, West Cambridge Site, Philippa Fawcett Drive, Cambridge, CB3 0AS, UK; [2]Department of Chemistry, University of Cambridge, Lensfield Road, Cambridge, CB2 1EW, UK; [3]Department of Life Sciences, Imperial College London, London; [4]Present address: Scientific Center for Optical and Electron Microscopy, ETH Zurich, Otto-Stern Weg 3, CH8093 Zurich, Switzerland; [5]Prothena Biosciences Inc, South San Francisco, California, 94080, USA; [6]Tanz Centre for Research in Neurodegenerative Diseases, University of Toronto, Toronto, Ontario M5T 2S8, Canada; [7]Cambridge Institute for Medical Research, Department of Clinical Neurosciences, University of Cambridge, Cambridge, CB2 0XY, UK; [8]Living Systems Institute, Department of Biosciences, University of Exeter, Exeter, EX4 4QD, UK;, SW7 2AZ, UK.

# both authors contributed equally

Corresponding author:

Gabriele S. Kaminski Schierle gsk20@cam.ac.uk

Abstract

Alpha-synuclein is known to bind to small unilamellar vesicles (SUVs) via its N-terminus which forms an amphipathic alpha-helix upon membrane interaction. Here we show that calcium binds to the C-terminus of alpha-synuclein, therewith increasing its lipid binding capacity. Using CEST-NMR we reveal that alpha-synuclein interacts with isolated synaptic vesicles with two regions, the N-terminus, already known from studies on SUVs, and additionally via its C-terminus, which is regulated by the binding of calcium. Indeed, dSTORM on synaptosomes shows that calcium mediates the localization of alpha-synuclein at the presynaptic terminal, and an imbalance in calcium or alpha-synuclein can cause synaptic vesicle clustering, as seen *ex vivo* and *in vitro*. This study provides a new view on the binding of alpha-synuclein to synaptic vesicles, which might also affect our understanding of synucleinopathies.

INTRODUCTION

Alpha-synuclein is a 140-residue protein, which constitutes three major protein regions, the N-terminus (aa 1-60), the non-amyloid-β component (NAC) region (aa 61-95), designated as the aggregation-prone region, and the C-terminus (aa 96-140). Alpha-synuclein is localized at the presynaptic terminals [1], and, while structurally disordered in solution [2,3], it also exists in a partially structured, membrane bound form. Indeed, alpha-synuclein can bind a variety of synthetic vesicles but displays a preference to bind to small, highly curved synthetic vesicles via its N-terminus [4–10]. NMR studies of alpha-synuclein binding to synaptic-like synthetic vesicles have shown that this interaction is primarily triggered by the N-terminal residues, but interactions propagate up to residue 98, with the central region of the protein (residues 65-97) having a key role in modulating the binding affinity to the membrane [11] and in promoting the clustering of synaptic vesicles [12].

Moreover, although it has been shown that the N-terminus of alpha-synuclein strongly interacts with lipid vesicles, it is important to note that so far all research on alpha-synuclein-lipid interactions has been carried out on synthetic lipid vesicles. It thus has yet to be shown how alpha-synuclein interacts with physiological synaptic vesicles which are clearly distinct from just lipid vesicles [13].

We hypothesised that calcium plays a role in the normal physiological function of alpha-synuclein since alpha-synuclein is primarily localised at the presynaptic terminals where high calcium fluctuations occur, ranging up to hundreds of μM [14,15], and since calcium has been previously shown to bind to alpha-synuclein at its C-terminus [16]. In addition, it is not clear what the calcium affinity to alpha-synuclein is, whether the C-terminus is equally amenable

75 to cations in the presence of synaptic vesicles, and how exposure to calcium would interfere
76 with the synaptic vesicle binding capacity of alpha-synuclein. To answer these questions, we
77 investigated firstly the calcium-binding properties of alpha-synuclein by NMR and Mass
78 spectrometry (MS). We then explored whether and how neutralisation of negative charges
79 on the C-terminus impacts on the interaction of alpha-synuclein with lipids and synaptic
80 vesicles. And finally, we tested whether the interaction of alpha-synuclein with synaptic
81 vesicles impacts on synaptic vesicle homeostasis and on alpha-synuclein aggregation and
82 toxicity related to Parkinson's disease (PD).
83
84 We show here that calcium interacts with the negatively charged C-terminus of alpha-
85 synuclein, having a K_D in the range of 21 μM. Using synaptic vesicles isolated from rat brain,
86 we performed chemical exchange saturation transfer (CEST) experiments in solution-state
87 NMR, and show that the C-terminus of alpha-synuclein has an increased tendency to interact
88 with synaptic vesicles upon calcium binding. In the presence of calcium, alpha-synuclein
89 exhibited specific clustering at the presynaptic terminal, which could be reversed by the
90 addition of a calcium chelator. In contrast, VAMP-2, a synaptic vesicle marker, was not
91 affected by these calcium changes. These findings suggest that the normal physiological role
92 of alpha-synuclein is to act as a calcium-dependent modulator of vesicle homeostasis at the
93 presynaptic terminal. Using ventral mesencephalic neurons, we further show that treatment
94 with dopamine, a neurotransmitter relevant in PD pathology, promoted the clustering of
95 alpha-synuclein positive vesicles. The latter was prevented by treatment with isradipine, a
96 voltage-gated calcium channel inhibitor. Furthermore, lowering either the levels of alpha-
97 synuclein or calcium prevented dopamine toxicity, indicating that both alpha-synuclein and
98 calcium levels need to be finely balanced. This study provides a new view on the binding of

alpha-synuclein to synaptic vesicles, which might also affect our understanding of synucleinopathies.

Results

Calcium increases the lipid binding of α-synuclein

We recorded ^{1}H-^{15}N heteronuclear single quantum correlation (HSQC) spectra of alpha-synuclein in solution NMR as a function of calcium concentration to determine the thermodynamics and structural nature of the calcium binding mechanism. An analysis of the spectra identified the C-terminus as the primary segment hosting chemical shift perturbations due to calcium binding. In addition, we found peak broadening for some residues in the NAC-region. Residues whose chemical shifts of the backbone amide N-H were mostly affected are aa 104, 107, 112, 119, 123, 124, 126, 127, 129, 130, 135, 136, 137 (Fig. 1a and Supplementary Fig. 1). In order to obtain information on the thermodynamics of the calcium affinity to alpha-synuclein, and since the number of calcium cations that are bound to alpha-synuclein was not known, we performed a global analysis by fitting the chemical shift perturbation using a multiple ligand model [17], which allows to estimate the binding constant when the exact number of ligands is not known. Similar models have also been used before to analyse multivalent interactions of other amyloidogenic proteins [18]. By performing best fit analysis we obtained a K_D of calcium affinity of 21 µM with the number of ligand cations, *L*, being 7.8 (Fig. 1b).

In order to provide further support on the number of ligand cations being bound to alpha-synuclein we performed electrospray ionisation mass spectrometry (MS) and found that at least six cations are bound to alpha-synuclein (Fig. 1c and Supplementary Table 1). We thus confirmed by two independent measurements that around 6-8 calcium ions can be bound to

123 alpha-synuclein providing further support of our determined K_D. A dissociation constant of
124 21 μM lies well within the range of physiological pre-synaptic calcium fluctuations, reaching
125 up to hundreds of μM in healthy neurons upon neuronal stimulation [14,15].
126
127 We then hypothesised that a neutralisation of negative charges on residues at the C-
128 terminus via dynamic binding of positively charged calcium ions facilitates the interaction of
129 alpha-synuclein with phospholipid membranes. To test this hypothesis, we incubated lipid
130 Folch extracts from bovine brain with alpha-synuclein in the presence of calcium and other
131 ions, including potassium, sodium and magnesium and measured the interaction of alpha-
132 synuclein with lipids via lipid pull-down. In the presence of calcium, the amount of alpha-
133 synuclein that precipitated with the lipids increased about 5-fold. Magnesium and a high
134 concentration of sodium ions also increased the amount of alpha-synuclein pulled down, but
135 not to the same extent as calcium (Fig. 1d and Supplementary Fig 2). A phase partitioning
136 assay further established that the hydrophobicity of alpha-synuclein increases upon calcium
137 addition, which is manifested by a higher abundance of the protein in the lipophilic
138 detergent phase (Supplementary Fig. 3).
139
140 **The C-terminus of α-synuclein binds to synaptic vesicles**
141 Having seen that calcium influences the binding of alpha-synuclein to lipids, we investigated
142 the interaction of alpha-synuclein with synaptic vesicles isolated from rat brain and its
143 dependence on calcium. Using measurements of chemical exchange saturation transfer
144 (CEST) in solution NMR [11,12] we probed the binding affinity along the protein sequence. This
145 analysis revealed that in the absence of calcium the interaction with synaptic vesicles was
146 strongest via the N-terminus. In the presence of calcium, however, the interaction of the C-

147 terminus and also for some residues of the NAC-region was increased (Fig. 2a), providing
148 further insight into how calcium can modify the C-terminus of alpha-synuclein and thereby
149 induce a stronger interaction with synaptic vesicles. To determine whether a calcium-
150 dependent lipid interaction is transient, and therefore dynamically regulated, we again
151 performed lipid pull down experiments. We show that, consistent with the fast exchange
152 regime observed in solution NMR, the calcium-dependent interaction of alpha-synuclein is
153 dynamic, as addition of the calcium chelator EGTA reverses calcium-mediated alpha-
154 synuclein lipid binding (Fig. 2b).
155
156 **α-synuclein is modulated by calcium at** presynaptic terminals
157 Synaptosomes, pinched off synapses that reseal as spherical droplets, were isolated from rat
158 brain and used to study the synaptic localization of alpha-synuclein in the presence or
159 absence of calcium. Using direct stochastic optical reconstruction microscopy (*d*STORM),
160 permitting sub-diffraction resolution imaging, we found that under normal physiological
161 conditions (low intracellular and high extracellular calcium concentrations) alpha-synuclein
162 was significantly polarized. This could be interpreted as if alpha-synuclein does not bind to
163 synaptic vesicles, however, our vitro data as well as data from previous reports [5–10] show a
164 strong binding of alpha-synuclein to synaptic vesicles. The polarization could therefore be
165 interpreted as a binding of alpha-synuclein to only a subset of synaptic vesicles (similar to
166 what has been indicated in Lee et al.[19]). When we depleted calcium in the extracellular
167 buffer by the addition of the calcium chelator EGTA and omitting calcium, alpha-synuclein
168 displayed a dispersed distribution throughout the synaptosome (Fig. 2c and Supplementary
169 Fig. 4).

170 The cluster sizes of the synaptosomal alpha-synuclein and synaptic vesicle associated protein
171 2 (VAMP2), were determined by cluster analysis and revealed that alpha-synuclein was
172 significantly more dispersed upon calcium starvation with EGTA, while calcium starvation
173 had no effect on the localization of VAMP2 (Fig. 2d). In order to address whether an increase
174 in intracellular calcium leads to a further clustering of alpha synuclein we stimulated the
175 synaptosomes with an extracellular solution at 70 mM KCl, which leads to membrane
176 depolarization and calcium influx via voltage-gated calcium channels. Our results show that
177 upon stimulation there is no further change in the distribution of alpha-synuclein throughout
178 the synaptosomes (Supplementary Fig. 5), suggesting that normal physiological calcium
179 concentrations are sufficient to induce alpha-synuclein clustering. The specificity of the
180 alpha-synuclein staining protocol was validated using synaptosomes derived from alpha-
181 synuclein knock-out mice (Supplementary Fig. 6). Furthermore, using synaptosomes from
182 wild type human alpha-synuclein overexpressing mice we see that alpha-synuclein loses its
183 ability to be specifically polarized under normal physiological conditions (Supplementary Fig.
184 7).
185
186 **α-synuclein and calcium regulate synaptic vesicle interaction**
187 Using NMR and synthetic lipids we have shown recently that alpha-synuclein is capable of
188 tethering vesicles and two protein regions were identified as participants in a double anchor
189 mechanism[12]. In order to quantify the dependencies of synaptic vesicle clustering on calcium
190 and alpha-synuclein, synaptic vesicles purified from rat brains were incubated with either 1
191 mM EGTA omitting calcium or 200 µM calcium and subsequently imaged using stimulated
192 emission depletion (STED) microscopy. For samples incubated with EGTA 88% of synaptic
193 vesicles were distributed as single vesicles, while 12% showed clustering with one or more

194 vesicles. However, in the presence of calcium the amount of single vesicles decreased to
195 84% and the number of multiple vesicles clustering together increased to 16%. This indicates
196 that, even for synaptic vesicles isolated from wild-type rat brain with endogenous levels of
197 alpha-synuclein present, calcium is a modulating factor of the cohesion between synaptic
198 vesicles. Next, we incubated synaptic vesicles with 200 µM of calcium and 50 µM of
199 recombinant alpha-synuclein, which, in combination with the endogenous alpha-synuclein,
200 leads to doubling of the level of alpha-synuclein present on synaptic vesicles [13]. Again, a
201 significant clustering of synaptic vesicles was observed with 81% distributed as single
202 synaptic vesicles and 19% as multiple vesicle clusters. Incubating synaptic vesicles with 50
203 µM of recombinant alpha-synuclein and 1 mM EGTA in combination, did however not
204 reverse synaptic vesicle clustering, indicating that the presence of an increased alpha-
205 synuclein level on its own can already induce synaptic vesicle clustering (Fig. 3a). A clustering
206 of synaptic vesicles upon incubation with 50 µM of alpha-synuclein was also observed via
207 transmission electron microscopy (Fig. 3b) and via combined confocal/STED imaging, the
208 latter verifying that synaptic vesicles colocalized with alpha-synuclein (Fig. 3c).
209
210 Next, we studied the behaviour of endogenous alpha-synuclein in ventral midbrain (VM)
211 neurons incubated with 100 µM dopamine. This system has previously been shown to
212 induce the formation of alpha-synuclein oligomers and to exhibit dopaminergic neuron-
213 specific toxicity [20–23]. VM neurons treated with dopamine for 72 h were stained against
214 endogenous alpha-synuclein and the synaptic vesicle protein synaptotagmin 1 and
215 subsequently imaged by *d*STORM. Upon incubation with dopamine, an increase in the area
216 of alpha-synuclein-positive puncta was observed, together with an increased size of
217 synaptotagmin 1 puncta and an increased colocalization of alpha-synuclein and

218 synaptotagmin 1 (Fig. 4a-c). We show that these dopamine-induced changes were reversed
219 by treating the cells with isradipine, a $Ca_V1.3$ calcium channel antagonist previously reported
220 to block dopaminergic neuron cell death in 1-Methyl-4-phenyl-1,2,3,6-tetrahydropyridine
221 (MPTP) and other neurotoxin-related Parkinson's disease models [24]. This demonstrates that
222 in the presence of endogenous alpha-synuclein levels calcium is necessary to induce synaptic
223 vesicle clustering, consistent with our observations from isolated synaptic vesicles. Since
224 isradipine was seen to significantly reduce clustering of alpha-synuclein, we tested if also
225 dopamine-induced cytotoxicity might be suppressed as a consequence of its action. Our data
226 show that dopamine-induced toxicity can be abolished both by the administration of
227 isradipine, or by knocking down of alpha-synuclein (Fig. 4d, Supplementary Fig. 8), indicating
228 that high levels of calcium and/or alpha-synuclein are key elements of neuronal toxicity.
229

230 **Calcium and synaptic vesicles affect α-synuclein aggregation**

231 Taken together our data indicate that calcium mediates the interaction of alpha-synuclein
232 and synaptic vesicles and that this has an effect in both physiological processes and under
233 conditions generating cellular toxicity. However, since both, either increased levels of alpha-
234 synuclein or calcium can induce cell death, we investigated whether calcium and synaptic
235 vesicles may influence the aggregation propensity of alpha-synuclein. To test this hypothesis,
236 we performed Thioflavin T (ThT) fluorescence assays of alpha-synuclein aggregation, and
237 analysed the effect of increased calcium in the presence and absence of synaptic vesicles
238 (Fig. 5a). The lag time for each condition was calculated from the averaged aggregation
239 curves by linear extension of the elongation phase. The nucleation rate (k_1) and the
240 elongation rate (k_2) were fitted using the Finke-Watzky equation for a two-step aggregation
241 mechanism [25]. This analysis clearly revealed that calcium aggravates alpha-synuclein

242 aggregation, showing a lag time decrease from 79 hours for 'EGTA only' to 4 hours for
243 'calcium only'. Accordingly, the nucleation rate was increased 2-fold in the presence of
244 calcium, and the elongation rate was increased 1.3-fold. Moreover, the amount of residual
245 monomer left at the end of the aggregation assay was significantly lower when calcium was
246 present, confirming the higher aggregation propensity of alpha-synuclein in the presence of
247 calcium. In the presence synaptic vesicles and calcium, we observed the highest nucleation
248 and elongation rate. In the absence of calcium, synaptic vesicles decreased the lag time from
249 79 hours to 44 hours and increased the nucleation rate 2-fold compared to the 'EGTA only'
250 group, which is in accordance with what has been reported for synthetic vesicles [17].
251 However, the elongation rate was not increased (Table 1).
252 Interestingly, alpha-synuclein fibrils formed at the end of the assay showed a different
253 morphology when synaptic vesicles were present during the aggregation process. When
254 alpha-synuclein was incubated in the presence of calcium and synaptic vesicles, alpha-
255 synuclein fibrils were shorter and showed aggravated bundling. In the presence of EGTA
256 significantly less fibrils were found. The few fibrils that could be found in the EGTA group
257 without synaptic vesicles were long and separated whereas the EGTA fibrils formed in the
258 presence of synaptic vesicles appeared to have an intermediate phenotype as they were still
259 bundled but longer than fibrils formed in the presence of synaptic vesicles and calcium (Fig.
260 5b). In order to confirm the presence of synaptic vesicles during the aggregation process we
261 show a TEM image of alpha-synuclein in the presence of synaptic vesicles at the beginning of
262 the aggregation experiment (Supplementary Fig. 9), as after seven days the vesicles cannot
263 be detected on the TEM anymore.
264
265 **Discussion**

266 The C-terminus of alpha-synuclein is negatively charged such that electrostatic interaction
267 can take place with cations [16]. In the past, however, research on such interactions has
268 predominantly been focused on metal ions as environmental factors inducing alpha-
269 synuclein aggregation [26–28]. Here, we focus on the interaction of alpha-synuclein with
270 physiological calcium, since at the presynaptic terminal, where alpha-synucleins primarily
271 resides, large fluctuations in calcium levels are known to occur [14,15]. We quantify and localise
272 the interactions of calcium with alpha synuclein using ^{1}H-^{15}N HSQC NMR and observe
273 significant chemical shift perturbations for a number of residues at the C-terminus of the
274 protein. Furthermore, significant peak broadening takes place in the NAC-region of alpha-
275 synucein in the presence of calcium. This can be interpreted either as a conformational
276 change in the NAC-region induced upon calcium binding at the C-terminus, or as an
277 interaction between multiple NAC-regions when individual alpha-synuclein molecules cluster
278 due to charge neutralisation. The affinity of calcium was found to be around 21 µM, which is
279 lower than reported for other multivalent cations [27]. While levels of calcium are in the tens
280 of nM range under resting conditions [29], it's concentration rises to several hundred µM
281 within microdomains during depolarization of neurons as a result of a concomitant calcium
282 influx via voltage-gated calcium channels [14,15]. In this context, the observed K_D of 21 µM
283 highlights the physiological relevance of the interaction between alpha-synuclein and
284 calcium.

285

286 CEST-NMR experiments, analysing the interaction of alpha-synuclein with synaptic vesicles
287 from rat brain, verified that in the presence of calcium the C-terminus has a higher affinity to
288 bind to synaptic vesicles. In a previous study [12] we have shown that the modes of binding of
289 the N-terminal and NAC-region of alpha-synuclein to small unilammelar vesicles (SUVs) of

290 DOPE:DOPS:DOPC (in 5:3:2 molar ratios) [11,12,30] are independent of each other. This degree
291 of independence suggested that the two regions can bind the same vesicle but also multiple
292 vesicles. We referred to this N-terminus and NAC-region binding of alpha-synuclein to SUVs
293 as double anchor mechanism. We now have characterised the binding of alpha-synuclein to
294 synaptic vesicles isolated from rat brain using CEST NMR, showing again that the strongest
295 binding occurs at the N-terminus and revealing an intermediate level of synaptic vesicle
296 interaction of the NAC-region and the C-terminus. Interestingly, upon addition of calcium
297 this binding via the C-terminus, and also for certain residues of the NAC-region, was found to
298 be increased. We refer to this as extended double anchor mechanism since the double
299 anchor has been extended to the C-terminus of alpha-synuclein. Our NMR data are
300 consistent with a study using site specific pyrene labelling of alpha-synuclein [31]. In that
301 study, it was shown that the N-terminus of alpha-synuclein binds to synthetic vesicles in the
302 absence of calcium, while the C-terminus does not. Upon calcium addition on its own, there
303 is a reduction in the polarity of the C-terminus, which suggests calcium binding. Moreover,
304 upon addition of synthetic vesicles a further reduction in the polarity was observed,
305 supporting a calcium-dependent lipid binding of the C-terminus. Summarising the above,
306 alpha-synuclein, in the presence of calcium, may act as an extended and strengthened
307 double anchor between synaptic vesicles, which could cause interaction in three different
308 ways: (i) the N- and C-terminus both tether to the same vesicle, (ii) the N-terminus binds to
309 one vesicle while the C-terminus binds to another vesicle via an extended double anchor
310 mechanism, or (iii) the N-terminus binds to synaptic vesicles, whereas the C-terminus binds
311 to the plasma membrane. Our observations, using synaptosomes, isolated synaptic vesicles
312 as well as ventral mesencephalic cells, suggest that calcium and alpha-synuclein can affect
313 vesicle pool homeostasis, either via promoting intervesicular interactions and/or via

314 tethering of synaptic vesicles to the plasma membrane, which could influence their
315 proximity to voltage gated calcium channels [32].
316
317 From the time of its discovery, alpha-synuclein has been known as a pre-synaptic protein,
318 suggesting a role in neurotransmitter release. It has been shown that the overexpression of
319 alpha-synuclein inhibits neurotransmitter release [33–37], while neurotransmitter release
320 appears facilitated in an alpha-synuclein knock-out model [38–41]. However, data are not
321 conclusive so far and a regulatory role rather than a direct role of alpha-synuclein in
322 exocytosis is still debated in the literature [42]. It has furthermore been suggested that alpha-
323 synuclein plays a role in endocytosis and in synaptic vesicle homeostasis (for detailed review
324 see [43]).
325
326 We show here, that in synaptosomes alpha-synuclein localization is dependent on calcium
327 since calcium depletion in the extracellular space does not lead to the polarization of alpha-
328 synuclein in the synaptosomes. It is interesting to note that we see little overlap between
329 alpha-synuclein and VAMP2 which could be interpreted as if alpha-synuclein does not bind
330 to synaptic vesicles at all. We do, however, not believe that this is the case for two main
331 reasons: First, all our in vitro data as well as data from others [5–10] show strong binding of
332 alpha-synuclein to synaptic vesicles. Second, it has been suggested that alpha-synuclein
333 binds to only a subset of synaptic vesicles [19], however, it may require further investigations
334 to fully determine which synaptic vesicles are positive for which synaptic vesicle protein.
335 We show that calcium as well as increased alpha-synuclein concentrations influence the
336 clustering of synaptic vesicles in vitro. Similar observations were made using synaptic
337 vesicle-mimics built of anionic phospholipids containing SNARE complex proteins [44]. The

338 authors showed that an increased alpha-synuclein concentration caused clustering of the
339 synaptic vesicle-mimics, which was dependent on the capacity of alpha-synuclein to bind to
340 lipids, as the lipid-binding deficient familial A30P alpha-synuclein mutant displayed a
341 decreased propensity to cluster vesicles. The authors report that also C-terminally truncated
342 alpha-synuclein can decrease vesicle clustering, which supports our hypothesis of an
343 extended double anchor binding mechanism of alpha-synuclein. The authors though indicate
344 that this is mediated via C-terminal binding of alpha-synuclein to VAMP2. In our study,
345 however, we do not observe clustering of VAMP2, suggesting that a VAMP2-independent
346 mechanism might be involved. Our proposed model of alpha-synuclein-dependent vesicle
347 clustering is further supported by recent studies demonstrating a decrease in synaptic
348 vesicle motility in neurons upon alpha-synuclein overexpression [45,46]. This is in line with our
349 observation that the overexpression of wild-type human alpha-synuclein reduced the
350 propensity of alpha-synuclein to be polarized upon calcium treatment in synaptosomes. It is
351 important to note though that not all of these calcium-controlled processes rely solely on
352 the presence of alpha-synuclein. This becomes clear from alpha-synuclein knock-out studies
353 in mice [41,47] but is further supported by the fact, that alpha-synuclein is expressed at late
354 stages of development, as shown for songbirds, for which alpha-synuclein becomes
355 upregulated during song acquisition [48].
356
357 Furthermore, we show here that dopamine toxicity known to induce alpha-synuclein
358 oligomerization [20–23,49] can be significantly reduced if either calcium levels are decreased,
359 using the $Ca_V1.3$ blocker isradipine, or if alpha-synuclein levels are reduced by knocking
360 down alpha-synuclein, suggesting that both calcium and alpha-synuclein need to be present
361 to convey dopamine-induced toxicity. This is in line with the findings that dopaminergic

362 neurons of the substantia nigra (SN) display a lower abundance of calcium-binding proteins
363 [50] and exhibit a calcium-driven pacemaking activity [51], putting them at higher risk for
364 calcium-mediated pathophysiology. Using in vitro aggregation assays, we see that calcium
365 clearly aggravates alpha-synuclein aggregation, in the presence or absence of synaptic
366 vesicles. We also observed an increase in nucleation when synaptic vesicles were added to
367 alpha-synuclein with EGTA, which is in line with the literature reporting that synthetic lipids
368 increase the rate of aggregation of alpha-synuclein [52]. Excess calcium can cause a
369 conformational change within the protein, such as by an exposure of the NAC-region upon
370 calcium binding, or simply via a change in the net charge of the protein, both facilitating the
371 propensity for aggregation. It is interesting to note though that alpha-synuclein fibrils
372 formed in vitro in the presence of isolated synaptic vesicles display a different morphology.
373
374 Understanding the above described role of alpha-synuclein in physiological or pathological
375 processes may impact strongly on the development of new therapeutics for PD.
376 Interestingly, antibodies targeted to the C-terminus of alpha-synuclein were demonstrated
377 to decrease intracellular alpha-synuclein pathology in animal models of synucleinopathy [53].
378 One such antibody, PRX002, is currently in phase 2 clinical development for Parkinson's
379 disease (ClinicalTrials.gov Identifier: NCT03100149). Also isradipine, which is used as calcium
380 channel blocker in heart diseases, may prove to be a valuable candidate to act against PD via
381 lowering intracellular calcium load [54,55] (ClinicalTrials.gov Identifier: NCT02168842).
382
383 **Methods**
384 **Purification of alpha-synuclein**

385 Human wild-type (WT) alpha-synuclein was expressed in Escherichia coli One Shot® BL21
386 STAR™ (DE3) (Invitrogen, Thermo Fisher Scientific, Cheshire, UK) cells using plasmid pT7-7
387 and purified using ion exchange on a HiPrep Q FF 16/10 anion exchange column (GE
388 Healthcare, Uppsala, Sweden) [56]. Alpha-synuclein was then further purified on a HiPrep
389 Phenyl FF 16/10 (High Sub) hydrophobic interaction column (GE Healthcare) [57]. Purification
390 was performed on an ÄKTA Pure (GE Healthcare, Sweden). Monomeric protein was dialyzed
391 against 20 mM Na_2HPO_4 pH 7.2 and stored at -80 °C. For experiments with dye-labelled
392 alpha-synuclein, the cysteine mutant N122C was purified and labeled with the ATTO-647N
393 dye (#05316, Sigma-Aldrich, Dorset, UK). For experiments with vesicles, monomeric human
394 WT alpha-synuclein was buffer exchanged using PD10 Desalting Columns (GE Healthcare)
395 into vesicle buffer (20 mM NaCl, 2.5 mM KCl, 25 mM HEPES, 30 mM Glucose, pH7.4 with
396 NaOH).
397
398 **Lipid pull down assay**
399 Lipid extract from bovine brain (Type I, Folch Fraction I; Sigma-Aldrich) was dissolved in lipid
400 buffer (1 mg/ml; 50 mM Tris + 100 mM NaCl, pH 7.4) and sonicated on ice using a Branson
401 SLPe sonicator (Branson Ultrasonic S.A., Geneva, Switzerland). The lipid was incubated with
402 2 µg of recombinant human alpha-synuclein with either KCl (50 mM), NaCl (150 or 300 mM),
403 $MgCl_2$ (1 mM) or $CaCl_2$ (1 mM), for 1 h at room temperature (RT). The different samples
404 were centrifuged for 20 min at 4000 x g at RT to obtain the pellet for analysis by Western
405 blot. The lipid pull down assay to prove reversibility of Ca^{2+}-dependent lipid binding was
406 done using post-incubation with EGTA (5 mM) for one 1 hour.

407 Western blot of alpha-synuclein was performed using 4-12% Bis-Tris gels (Life Technologies),
408 the protein was transferred onto 0.2 µm Millipore PVDF membrane (Fisher Scientific,

409 Loughborough, UK) and subsequently fixed using 0.4% formaldehyde (Sigma-Aldrich) and
410 0.1% glutaraldehyde (Sigma-Aldrich). The primary mouse anti-alpha-synuclein antibody
411 LB509 (LB509, 1:1000 dilution, Life Technologies) and an enhanced chemoluminescence
412 (ECL)-horse radish peroxidase (HRP) conjugated secondary antibody (NA931, 1:1000 dilution,
413 GE Healthcare) and SuperSignal West Femto Chemiluminescent Substrate (Thermo Fisher
414 Scientific, Epsom, UK) were used to probe the membrane, which was exposed using a G:BOX
415 (Syngene, Cambridge, UK).
416
417 **Animals**
418 Animals were bred and supplied by Charles River UK Ltd., Scientific, Breeding and Supplying
419 Establishment, registered under Animals (Scientific Procedures) Act 1986, and AAALAC
420 International accredited. All animal work conformed to guidelines of animal husbandry as
421 provided by the UK Home Office. Animals were sacrificed under schedule 1; procedures that
422 do not require specific Home Office approval. Animal work was approved by the NACWO
423 and University of Cambridge Ethics Board.
424
425 **Synaptic vesicles, synaptosomes and cell cultures**
426 Isolation of synaptic vesicles (SV) was performed as previously described [58]. Brains were
427 dissected from WT Sprague-Dawley rats, two brains were used per SV preparation. The
428 vesicle pellet was resuspended in 200 µL of vesicle buffer (20 mM NaCl, 2.5 mM KCl, 25 mM
429 HEPES, 30 mM Glucose, pH 7.4 with NaOH) and snap-frozen in aliquots in liquid nitrogen
430 before being stored at -80°C. SVs had a protein concentration of 3.3 mg/mL.
431 Synaptosomes were prepared from WT Sprague-Dawley adult rat brains as described
432 previously [59]. Briefly, the brain was homogenized in a glass-Teflon EUROSTAR20

433 homogeniser (IKA, Oxon, UK) in homogenizing buffer made from sucrose/EDTA buffer (320
434 mM sucrose, 1 mM EDTA, 5 mM Tris, pH 7.4) with 50 mM DTT, using 10 strokes at 800 rpm.
435 Synaptosomes were isolated using 3 % - 23 % Percoll gradients. The synaptosome containing
436 fractions were pooled and resuspended in extracellular buffer solution (20 mM sodium
437 HEPES, 130 mM NaCl, 5 mM $NaHCO_3$, 1.2 mM Na_2HPO_4, 1mM $MgCl_2$, 10 mM glucose, 5 mM
438 KCl, 2.5 mM $CaCl_2$, pH 7.4). Synaptosomes were loaded onto 8 well glass bottom µ-slides
439 (ibidi GmbH, Munich, Germany), which were cleaned with 1 M KOH and coated with poly-L-
440 lysine 0.01 % solution (mol wt 70.000 – 150.000, Sigma-Aldrich) over night at 4°C.
441 Synaptosomes were stimulated for 30 min at 37 °C with extracellular solution made at either
442 5 mM KCl + 2.5 mM $CaCl_2$, 5 mM KCl + 1 mM EGTA or 70 mM KCl + 2.5 mM $CaCl_2$.
443 Synaptosomes were then fixed with 4 % formaldehyde (Sigma-Aldrich) in PBS. Fixation was
444 quenched by washing with 0.1 M glycine in PBS for 5 min.

445 Ventral mesencephalic (VM) neurons were dissected from E14 Sprague-Dawley rat embryos.
446 In brief, VM tissue was incubated in 0.1% trypsin (Worthington Biochemical Corporation,
447 Lakewood, USA) and 0.05% DNase (Sigma-Aldrich) in DMEM (Sigma-Aldrich) for 20 min at
448 37°C. Cells were washed 4 times with 0.05% DNase in DMEM and triturated until a single cell
449 suspension was reached. Neurons were seeded at 100,000 cells/well in LabTek II chambered
450 coverglass (Thermo Fisher Scientific) coated with poly-L-lysine 0.01 % solution (mol wt
451 70.000 - 150.000, Sigma-Aldrich). Neurons were kept in DMEM with 10 % fetal bovine serum
452 (FBS, 10270-106, Gibco®) for 3 hours, then media was changed to Neurobasal media Gibco®
453 supplemented with 2 % B27 Gibco®, 0.5 mM GlutaMax Gibco® and 1 % antibiotic-
454 antimycotic Gibco® (all Thermo Fisher Scientific). Neurons were used at days in vitro (DIV)
455 14. Fixation was performed for 10 min using 4 % formaldehyde (Sigma-Aldrich) in PBS
456 containing 4 % sucrose, 5 mM $MgCl_2$ and 10 mM EGTA.

457 Human neuroblastoma cells (SH-SY5Y) were obtained from the European Collection of Cell
458 Cultures (ECACC, Sigma-Aldrich) and grown in a 1:1 minimal essential medium (MEM)
459 (Sigma-Aldrich) and nutrient mixture F-12 Ham (Sigma-Aldrich) supplemented with 15 % FBS
460 Gibco®, 1 % non-essential amino-acids Gibco®, 2 mM GlutaMAX Gibco® and 1 % antibiotic-
461 antimycotic Gibco® (all Thermo Fisher Scientific). Cells were plated at 5,000 cells/well in
462 Nunc MicroWell 96 well plates (Thermo Fisher Scientific) for cytotoxicity assays and at
463 700,000 cells/dish in 48 mm dishes (Nunc A/A) for western blotting studies. Cells were
464 tested for mycoplasma contamination.

465 Treatment of cells was performed using 100 µM dopamine (100x stock solution in water,
466 freshly prepared, Sigma-Aldrich) or 100 µM dopamine + 5 µM isradipine (1000x stock
467 solution in DMSO, Sigma-Aldrich). Control cells received 0.1 % DMSO and 1 % water,
468 respectively. Isradipine treatment was carried out 30 min early to dopamine treatment.
469 After 72 hours of incubation, cells were fixed or underwent cytotoxicity assay using the cell
470 cytotoxicity assay kit, ab112118 (Abcam, Cambridge, UK) according to manufacturer's
471 instructions. Absorbance intensity was measured at 570 nm and 605 nm, with the ratio
472 OD570/OD605 being proportional to the number of viable cells.

473

474 **Solution NMR**

475 In order to probe the structure and thermodynamics of calcium binding with alpha-synuclein
476 at a residue specific level, we employed a series of ^{1}H-^{15}N HSQC experiments using different
477 concentrations of Ca^{2+} (0.0 mM to 3.6 mM) and a fixed concentration of alpha-synuclein
478 (200 µM). NMR experiments were carried out at 10 °C on a Bruker spectrometer operating
479 at ^{1}H frequencies of 800 MHz equipped with triple resonance HCN cryo-probe. The ^{1}H-^{15}N

480 HSQC experiments were recorded using a data matrix consisting of 2048 (t_2, ^{1}H) × 220 (t_1,

481 ^{15}N) complex points. Assignments of the resonances in ^{1}H-^{15}N-HSQC spectra of alpha-

482 synuclein were derived from our previous studies [11].

483 The chemical shift perturbation in the ^{1}H-^{15}N HSQC spectra was analysed using a weighting

484 function:

$$\Delta\delta = \sqrt{\frac{1}{2}(\delta_H^2 + 0.15\delta_N^2)}$$

485 These provide the fraction of bound alpha-synuclein, χ_B, which is calculated as:

$$\chi_B = \frac{\Delta\delta_{obs}}{\Delta\delta_{sat}}$$

486 Where the $\Delta\delta_{obs}$ is the variation of the chemical shifts of a peak of alpha-synuclein that is

487 observed at a given $[Ca^{2+}]$, and $\Delta\delta_{sat}$ is the maximum variation obtained at saturation with

488 an excess of calcium. χ_B was calculated as a function of $[Ca^{2+}]$ for every peak of the protein,

489 and a global χ_B was used to include the chemical shift variations from all the peaks

490 associated with the major perturbations in the presence of calcium. We then used a fitting

491 procedure based on a binding model describing χ_B as a function of the total $[Ca^{2+}]$ [17]

492 $$\alpha syn^U + Ca^{2+}{}_L \rightleftarrows \alpha syn^B(Ca^{2+})_L \quad (1)$$

493 Where αsyn^U and αsyn^B indicate free and calcium bound alpha-synuclein, L indicates the

494 number of Ca^{2+} interacting with one alpha-synuclein molecule. The equilibrium dissociation

495 constant from this model is given by

496 $$K_D = \frac{[\alpha syn^U][Ca^{2+}{}_L]}{[\alpha syn^B(Ca^{2+})_L]} \quad (2)$$

497 the overall concentration of alpha-synuclein in this equilibrium is given by

498 $$[\alpha syn] = [\alpha syn^U] + [\alpha syn^B(Ca^{2+})_L] \quad (3)$$

499 and the overall concentration of Ca^{2+} is given by

500 $$[Ca^{2+}] = L([Ca^{2+}]_L + [\alpha syn^B(Ca^{2+})_L]) \quad (4)$$

501 Leading to the following fitting function

$$\chi_B = \frac{[\alpha syn] + \left[\frac{Ca^{2+}}{L}\right] + K_D - \sqrt{\left([\alpha syn] + \left[\frac{Ca^{2+}}{L}\right] + K_D\right)^2 - \frac{4[\alpha syn][Ca^{2+}]}{L}}}{2[\alpha syn]}$$

502

503 **Chemical exchange saturation transfer (CEST) NMR**

504 CEST NMR is widely used to probe the interaction of amyoloidogenic proteins[60,61]. Here we
505 employed CEST measurements [11,62–65] to directly probe the equilibrium between vesicle
506 unbound and bound states of alpha-synuclein. CEST has enhanced characteristics compared
507 to standard heteronuclear correlation spectroscopy in probing the details of the equilibrium
508 between NMR visible (unbound alpha-synuclein) and NMR invisible (vesicle bound alpha-
509 synuclein). These include a significant sensitivity at low vesicle:protein ratios and the
510 avoidance of other factors that may influence the transverse relaxation rates of the protein
511 resonances. CEST experiments were carried out at 10 °C on a Bruker spectrometer operating
512 at ^{1}H frequencies of 800 MHz equipped with triple resonance HCN cryo-probe. The
513 measurements were based on ^{1}H-^{15}N HSQC experiments by applying constant wave
514 saturation of 400 Hz in the ^{15}N channel. A series of large offsets was employed (-9, -7, -5, -4,
515 -3, -1.5, 0, 1.5, 3, 4, 5, 7, 9 kHz), and additional spectrum, saturated at -100 kHz, was
516 recorded as a reference. The saturation of the bound state is transferred to the free state *via*
517 the conformational exchange of these two states, resulting in the saturation of the peak

518 intensities in the visible unbound state. The CEST experiments were recorded using a data
519 matrix consisting of 2048 (t_2, ^1H) × 220 (t_1, ^{15}N) complex points.
520
521 **Mass spectrometry (MS) for the determination of alpha-synuclein-Ca complexes**
522
523 Samples of 10 µM wild-type alpha-synuclein in Tris buffer (20 mM, pH 7.4) were diluted in
524 50% methanol/ 50% dH_2O (v/v) to a final concentration of 2 µM. Samples containing 3.6 mM
525 $CaCl_2$ were also prepared as described below. Stock solution of $CaCl_2$ was added to the
526 alpha-synuclein sample and gently mixed with a micropipette, and then incubated for 15 min
527 at room temperature. The sample was then diluted with 50% methanol/ 50% dH_2O (v/v) to a
528 final protein concentration of 2 µM before MS analysis. The effect of formic acid
529 concentration on the MS signal was also investigated: for that reason, the previous samples
530 were also prepared with formic acid to final concentrations of 0.01, 0.1 & 1% (v/v). Samples
531 were infused into a Synapt G2-Si mass spectrometer (Waters, USA) using a syringe pump
532 (CorSolutions, USA) at a flow rate of 3.5 µL/min. Source temperature 80 ^oC, cone voltage 30
533 V, desolvation temperature 250 ^oC, trap collision energy 4.0 V, transfer collision energy 4.0
534 V, Source pressure 7.7x10^-6 bar, Trap pressure 8.8x10^-6 bar, IMS cell pressure 2.6x10^-7
535 bar, Transfer pressure 8.7x10^-6 bar. All data were collected in positive ion mode.
536
537 **Immunofluorescence**
538 Blocking and permeabilization were performed using 5 % serum and 0.01 % digitonin in
539 phosphate buffered saline (PBS) for 1 h. Primary antibodies were incubated for 1 hour,
540 followed by 4 washes with PBS. Secondary antibodies were incubated for 10 min, followed
541 by 4 washes with PBS. For staining of synaptosomes no digitonin was used, instead all

542 solutions contained 0.05% Tween-20. Samples were kept in PBS containing 5 mM sodium
543 azide (Sigma-Aldrich).

544 For STED imaging of synaptic vesicles, two primary antibodies, targeting the two most
545 abundant SV proteins [13] synaptophysin (101002, 1:750 dilution, SYnaptic SYstems,
546 Goettingen, Germany) and VAMP2 (104202, 1:750 dilution, SYnaptic SYstems) were used in
547 purpose of improved signal to noise ratio. A secondary anti-rabbit antibody conjugated with
548 ATTO-647N (40839, 1:100 dilution, Sigma-Aldrich) was used to detect both primary
549 antibodies simultaneously. For combined confocal/STED imaging of synaptic vesicles and
550 alpha-synuclein, vesicles were stained with a primary antibody for synaptotagmin 1 (105103,
551 1:500 dilution, SYnaptic SYstems) and a secondary anti-rabbit antibody conjugated with
552 Alexa-488 (18772, 1:100 dilution, Sigma-Aldrich).

553 Synaptosomes were stained for alpha-synuclein (D37A6 XP®, 1:500 dilution, rabbit, Cell
554 Signalling, Danvers, US) and VAMP2 (104211, 1:500 dilution, mouse, SYnaptic SYstems,
555 Goettingen, Germany). As secondary antibodies anti-rabbit Alexa Fluor®647 (ab150067,
556 1:200 dilution, Abcam) and anti-mouse Alexa Fluor®568 (ab175700, 1:200 dilution, Abcam)
557 were used.

558 VM neurons were stained for alpha-synuclein (ab6162, 1:300 dilution, sheep, Abcam) and
559 synaptotagmin 1 (105103, 1:500 dilution, rabbit, SYnaptic SYstems). As secondary antibodies
560 anti-sheep Alexa Fluor®647 (A21448, 1:200 dilution, Life Technologies) and anti-rabbit Alexa
561 Fluor®568 (A11036, 1:1000 dilution, Life Technologies) were used. Postfixation was
562 performed with 4 % formaldehyde (Sigma-Aldrich) for 10 min to minimize the occurrence of
563 detached fluorophore which would interfere with *d*STORM imaging.

564

565 **TEM, STED and *d*STORM**

566 For *transmission electron microscopy (TEM)* imaging of synaptic vesicles 1 µL of SVs (3.3
567 mg/mL) were incubated in 50 µL of vesicle buffer at 37 °C with and without 50 µM
568 monomeric alpha-synuclein for 4 days without shaking. 10 µL of each sample was incubated
569 on glow-discharged carbon coated copper grids for 1 min before washing twice with dH_2O.
570 2% uranyl acetate was used to negatively stain the samples for 30 s before imaging on the
571 Tecnai G2 80-200kv TEM at the Cambridge Advanced Imaging Centre.

572 For stimulated emission depletion (STED) imaging 0.5 µL of SVs (3.3 mg/mL) in 100 µL vesicle
573 buffer were incubated with either 200 µM $CaCl_2$ or 1 mM EGTA, with or without 50 µM WT
574 unlabelled alpha-synuclein. The mixture was taken up and down a 30 G needle to disperse
575 the SV, before incubating at 37°C for 24 hours using Lo-Bind Protein Eppendorf tubes. 8 well
576 glass bottom µ-slides (ibidi GmbH, Munich, Germany) were coated with Biotin-PEG-
577 cholesterol according to the protocol described previously [66] and synaptic vesicles were
578 allowed to adhere for 1 hour at RT. SVs were fixed with 4% formaldehyde (Sigma-Aldrich) in
579 PBS for 30 minutes and washed three times with PBS, staining was performed as described
580 above. For combined confocal/STED imaging 50 µM human WT alpha-synuclein was
581 complemented with 10% of alpha-synuclein N122C mutant labeled with ATTO-647N dye
582 (05316, Sigma-Aldrich). This allowed direct imaging of alpha-synuclein, while synaptic
583 vesicles were immunolabelled as described above. STED imaging was performed on a home-
584 built pulsed STED microscope [12]. STED excitation (λ_{exc} = 640 nm) and depletion (λ_{depl} = 765
585 nm) were generated from the same titanium sapphire oscillator operating at 765 nm. The
586 beam was divided between two paths. In the excitation path, a supercontinuum was
587 generated by pumping a photonic crystal fiber (SCG800, NKT photonics, Cologne, Germany)
588 and the excitation wavelength was selected by a bandpass filter (637/7 BrightLine HC,

589 Semrock, NY, USA). Excitation and depletion pulse lengths were stretched to 56 ps and 100
590 ps respectively through propagation in SF66 glass and polarization maintaining single mode
591 fibers. The depletion beam was spatially shaped into a vortex beam by a spatial light
592 modulator (X10468 02, Hamamatsu Photonics, Hamamatsu City, Japan) and the beams were
593 recombined using a spatial light modulator. Imaging was performed using a commercial
594 point scanning microscope (Abberior Instruments, Göttingen, Germany) comprising the
595 microscope frame (IX83, Olympus, Shinjiuku, Japan), a set of galvanometer mirrors (Quad
596 scanner, Abberior Instruments) and a detection unit. A 100X/1.4 NA oil immersion objective
597 (UPLSAPO 100XO, Olympus) and the Inspector software was used for data acquisition
598 (Andreas Schönle, Max Planck Institute for Biophysical Chemistry, Göttingen, Germany).
599 Fluorescence emission was descanned, focused onto a pinhole and detected using an
600 avalanche photodiode (SPCM-AQRH, Excelitas Technologies. Waltham, USA). A field of view
601 of 20 x 20 μm^2 and 20 nm pixel size was used. Confocal images of ATTO488 labeled vesicles
602 were correlated with STED images. Images were acquired on the same system as described
603 above. Fluorescence excitation at 488 nm (Cobolt 06-MLD, Cobolt, Solna, Sweden).
604 Fluorescence emission was filtered by a dichroic mirror (ZT594rdc, Chroma, Olching,
605 Germany) and a bandpass filter (FF01-550/88-25, Semrock). 6 images were analysed per
606 condition for 3 experiments.
607
608 Direct stochastic optical reconstruction microscopy (dSTORM) was performed as previously
609 described [67]. Briefly, imaging was performed on a Nikon TE inverted microscope using a
610 100x, 1.49 NA TIRF objective lens (Nikon UK Ltd.). Excitation at 640 nm (Toptica Photonic AG,
611 Graefelfing, Germany) was used for Alexa Fluor®647 and 561 nm (Oxxius SLIM-561) for Alexa
612 Fluor®568. Laser beams were collimated and combined by dichroic mirrors and expanded to

613 illuminate the sample for widefield fluorescence microscopy. A 405 nm (120 mW)
614 (Mitsubishi Electronics Corp., Tokyo, Japan) laser was used as reactivation source. The
615 fluorescence light in the detection path was separated from the illumination light by a
616 dichroic filter cube (Semrock multi-edge dichroic Di01-R405/488/561/635-25x36 followed by
617 a FF01-446/523/600/677-25 filter, Semrock, Rochester NY, USA) and was subsequently
618 filtered further using additional band-pass filters (Semrock BP-607/35-25 or BP-642/35-25
619 for Alexa Fluor®647 and Alexa Fluor®568 respectively). An electron-multiplying charge-
620 coupled device (EM-CCD) camera (Andor iXon DV887 ECS-BV, Andor, Belfast, Northern
621 Ireland) was used for detection. The excitation intensity was 2 kW/cm^2 for the 640 nm laser
622 and 5 kW/cm^2 for the 561 nm laser. Single-molecule photoswitching of the Alexa Fluor® 647
623 and Alexa Fluor® 568 were performed in thiol-containing switching buffer [68] using 100 mM
624 mercaptoethylamine (MEA) in PBS, adjusted to pH 10 using 1 M KOH. Imaging was
625 performed in highly inclined (HiLo) illumination mode [69]. 16 000 image frames with exposure
626 times between 7.18 and 20 ms were recorded and subsequently reconstructed using either
627 rapidSTORM 3.3 [70] or the open source rainSTORM software developed in-house [71] written in
628 MATLAB (The MathWork Inc., Natick, USA). Image overlays were assembled in FIJI [72],
629 experiments described were repeated at least three times and all images were processed as
630 described in the following section.

631

632 **Image Analysis**

633 Western blots were analysed in FIJI [72]. For the analysis of synaptosomal alpha-synuclein and
634 VAMP2 distribution, individual synaptosomes and their associated fluorophore localizations
635 as found by rapidSTORM were segmented from the aligned overlay-images using a custom-
636 written Matlab script. From the data files, the size for alpha-synuclein distribution and

637 VAMP2 distribution per synaptosomes were measured using a cluster analysis algorithm
638 with Ripley's K function as cluster size metric [73]. In short, the algorithm measures the
639 Euclidian distances between each localization with every other one. A histogram of the
640 distances is then generated and normalized by a histogram as expected from randomly
641 placed localizations at the same mean density. The maximum distance value of the
642 normalized histogram then yields a measure for the radius of the localization clusters. For
643 image analysis of synaptic vesicles, the spot detector plugin of the image analysis software
644 ICY was used to identify vesicles [74,75], followed by analysis using an in-house MATLAB script
645 to calculate the number of vesicles within a 250 nm radius (see code for image analysis of
646 synaptic vesicle STED images in Supplementary Methods). Analysis of alpha-synuclein and
647 synaptotagmin 1 in ventral midbrain neurons was performed using the particle analysis
648 plugin of the image analysis software FIJI [72]. For colocalisation analysis, the Coloc 2 plugin
649 was used [76], based on Pearson's correlation analysis.
650

651 **ThT Assay and SEC-HPLC quantification of alpha-synuclein monomer**

652

653 The aggregation of alpha-synuclein was measured by Thioflavin T (ThT) assay. Briefly, 10 µM
654 ThT was incubated with 100 µL of 100 µM alpha-synuclein with 2.5 mM $CaCl_2$ or 1 mM EGTA
655 with and without 1 µL 3.3 mg/mL SV. Assays were performed in non-binding, clear bottom,
656 black 96-well plates (PN 655906 Greiner Bio-One GmbH, Essen, Germany) which were sealed
657 with an Ampliseal transparent microplate sealer (Greiner Bio-One GmbH). Plates were
658 incubated with orbital shaking at 300 rpm at 37 °C and the readings of ThT fluorescence
659 intensity at 486 nm were collected every 16 min for 300 cycles in the top excitation/emission
660 mode at a focal height of 5.5 mm. Excitation was set at 440 nm with 2 flashes using 10% of

661 the excitation light (Envision 2104 Multilabel Reader, PerkinElmer, Turku, Finland).
662 Experiments were repeated three times with six replicates for each condition. The lag time
663 was calculated by extension of a linear fit to the elongation phase, passing through the
664 baseline using the equation: y = a + b * x. k_1 (nucleation rate constant) and k_2 (growth rate
665 constant) were calculated from the Finke-Watzky two-step model fitted to sigmoidal curves
666 of ThT fluorescence [25,77] using the equation below:

$$[B]_t = [A]_0 - \frac{\frac{k_1}{k_2} + [A]_0}{1 + \frac{k_1}{k_2[A]_0}\exp(k_1 + k_2\,[A]_0 t)}$$

667 , where $[B]_t$ is the concentration of product, $[A]_0$ is the concentration of reactant at time 0 h,
668 k_1 is the nucleation rate constant and k_2 the elongation rate constant.
669 10 µL samples of alpha-synuclein fibrils were taken from each condition of the ThT assay and
670 imaged by TEM as described above. Then, samples were removed from the wells and
671 centrifuged at 21,100 x g for 1 hour at RT to pellet fibrils and oligomers. The supernatant
672 was removed for quantitative analysis by size exclusion chromatography (SEC). SEC analysis
673 was performed on Agilent 1260 Infinity HPLC system (Agilent Technologies LDA UK Limited,
674 Stockport, UK) equipped with an autosampler and a diode-array detector using BioSep-SEC-
675 2000s column (Phenomenex, Macclesfield, UK) in phosphate-buffered saline (Gibco® PBS,
676 Thermo Fischer Scientific) at 1 mL/min flow-rate. The elution profile was monitored by UV
677 absorption at 220 and 280 nm. Remaining monomer concentration of alpha-synuclein was
678 calculated from a calibration curve. Remaining monomer concentration for samples with SVs
679 could not be calculated due to the presence of contaminating SV proteins obscuring the
680 monomeric alpha-synuclein chromatographic profile.
681
682 **Statistics**

683 Statistical analysis was performed using GraphPad Prism 6.07 (GraphPad Software, Inc., La
684 Jolla, CA, USA). Values are given as mean ± sem unless otherwise stated. Either two-tailed t-
685 test or one-way ANOVA with Tukey's post hoc correction were used as indicated.
686 Significance was considered at $p < 0.05$.

687

688 **Data availability**

689 All relevant data are available from the authors.

690

691 **References**

692 1. Maroteaux, L., Campanelli, J. T. & Scheller, R. H. Synuclein: a neuron-specific protein
693 localized to the nucleus and presynaptic nerve terminal. *J. Neurosci.* **8,** 2804–2815
694 (1988).
695 2. Weinreb, P. H., Zhen, W., Poon, A. W., Conway, K. A. & Lansbury, P. T. NACP, a protein
696 implicated in Alzheimer's disease and learning, is natively unfolded. *Biochemistry* **35,**
697 13709–13715 (1996).
698 3. Theillet, F.-X. *et al.* Structural disorder of monomeric α-synuclein persists in
699 mammalian cells. *Nature* **530,** 45–50 (2016).
700 4. Chandra, S., Chen, X., Rizo, J., Jahn, R. & Südhof, T. C. A broken α-helix in folded α-
701 synuclein. *J. Biol. Chem.* **278,** 15313–15318 (2003).
702 5. Georgieva. Membrane-Bound Alpha-Synuclein Forms an Extended Helix: Long-
703 Distance Pulsed ESR Measurements Using Vesicles, Bicelles, and Rod-Like Micelles. *J*
704 *Am Chem Soc* **130,** 12856–12857 (2008).
705 6. Jao, C. C., Hegde, B. G., Chen, J., Haworth, I. S. & Langen, R. Structure of membrane-
706 bound alpha-synuclein from site-directed spin labeling and computational refinement.

707 *Proc. Natl. Acad. Sci. U. S. A.* **105,** 19666–19671 (2008).

708 7. Bodner, C. R., Dobson, C. M. & Bax, A. Multiple Tight Phospholipid-Binding Modes of
709 α-Synuclein Revealed by Solution NMR Spectroscopy. *J. Mol. Biol.* **390,** 775–790
710 (2009).

711 8. Middleton, E. R. & Rhoades, E. Effects of curvature and composition on α-synuclein
712 binding to lipid vesicles. *Biophys. J.* **99,** 2279–2288 (2010).

713 9. Trexler, A. J. & Rhoades, E. α-Synuclein binds large unilamellar vesicles as an extended
714 helix. *Biophysics (Oxf).* **48,** 2304–2306 (2010).

715 10. Ulmer, T. S., Bax, a., Cole, N. B. & Nussbaum, R. L. Structure and Dynamics of Micelle-
716 bound Human α-Synuclein. *J. Biol. Chem.* **280,** 9595–9603 (2005).

717 11. Fusco, G. *et al.* Direct observation of the three regions in α-synuclein that determine
718 its membrane-bound behaviour. *Nat. Commun.* **5,** 1–8 (2014).

719 12. Fusco, G. *et al.* Structural basis of synaptic vesicle assembly promoted by α-synuclein.
720 *Nat. Commun.* **7,** 12563 (2016).

721 13. Takamori, S. *et al.* Molecular Anatomy of a Trafficking Organelle. *Cell* **127,** 831–846
722 (2006).

723 14. Llinás, R., Sugimori, M. & Silver, R. B. Microdomains of high calcium concentration in a
724 presynaptic terminal. *Science* **256,** 677–679 (1992).

725 15. Schneggenburger, R. & Neher, E. Intracellular calcium dependence of transmitter
726 release rates at a fast central synapse. *Nature* **406,** 889–893 (2000).

727 16. Nielsen, M. S., Vorum, H., Lindersson, E. & Jensen, P. H. Ca2+ Binding to α-Synuclein
728 Regulates Ligand Binding and Oligomerization. *J. Biol. Chem.* **276,** 22680–22684
729 (2001).

730 17. Galvagnion, C. *et al.* Lipid vesicles trigger α-synuclein aggregation by stimulating

731 primary nucleation. *Nat. Chem. Biol.* **11,** 229–234 (2015).

732 18. Algamal, M., Milojevic, J., Jafari, N., Zhang, W. & Melacini, G. Mapping the Interactions
733 between the Alzheimer's Aβ-Peptide and human serum albumin beyond domain
734 resolution. *Biophys. J.* **105,** 1700–1709 (2013).

735 19. Lee, S. J., Jeon, H. & Kandror, K. V. ??-Synuclein is localized in a subpopulation of rat
736 brain synaptic vesicles. *Acta Neurobiol. Exp. (Wars).* **68,** 509–515 (2008).

737 20. Outerio, T. F. *et al.* Dopamine-induced conformational changes in alpha-synuclein.
738 *PLoS One* **4,** 1–11 (2009).

739 21. Conway, K. A., Rochet, J. C., Bieganski, R. M. & Lansbury, P. T. Kinetic stabilization of
740 the α-synuclein protofibril by a dopamine-α-synuclein adduct. *Science* **294,** 1346–
741 1349 (2001).

742 22. Rekas, A. *et al.* The structure of dopamine induced α-Synuclein oligomers. *Eur.*
743 *Biophys. J.* **39,** 1407–1419 (2010).

744 23. Mosharov, E. V. *et al.* Interplay between Cytosolic Dopamine, Calcium, and α-
745 Synuclein Causes Selective Death of Substantia Nigra Neurons. *Neuron* **62,** 218–229
746 (2009).

747 24. Chan, C. S. *et al.* 'Rejuvenation' protects neurons in mouse models of Parkinson's
748 disease. *Nature* **447,** 1081–1086 (2007).

749 25. Watzky, M. A. & Finke, R. G. Transition metal nanocluster formation kinetic and
750 mechanistic studies. A new mechanism when hydrogen is the reductant: Slow,
751 continuous nucleation and fast autocatalytic surface growth. *J. Am. Chem. Soc.* **119,**
752 10382–10400 (1997).

753 26. Binolfi, A. *et al.* Interaction of α-synuclein with divalent metal ions reveals key
754 differences: A link between structure, binding specificity and fibrillation

755 enhancement. *J. Am. Chem. Soc.* **128,** 9893–9901 (2006).

756 27. Lu, Y., Prudent, M., Fauvet, B., Lashuel, H. a & Girault, H. H. Phosphorylation of alpha-
757 Synuclein at Y125 and S129 alters its metal binding properties: implications for
758 understanding the role of alpha-Synuclein in the pathogenesis of Parkinson's Disease
759 and related disorders. *ACS Chem Neurosci* **2,** 667–675 (2011).

760 28. Uversky, V. N., Li, J. & Fink, A. L. Metal-triggered structural transformations,
761 aggregation, and fibrillation of human α-synuclein: A possible molecular link between
762 parkinson's disease and heavy metal exposure. *J. Biol. Chem.* **276,** 44284–44296
763 (2001).

764 29. Maravall, M., Mainen, Z. F., Sabatini, B. L. & Svoboda, K. Estimating Intracellular
765 Calcium Concentrations and Buffering without Wavelength Ratioing. *Biophys. J.* **78,**
766 2655–2667 (2000).

767 30. Fusco, G. *et al.* Structural basis of membrane disruption and cellular toxicity by alpha-
768 synuclein oligomers. Science **358,** 1440–1443 (2017).

769 31. Tamamizu-Kato, S. *et al.* Calcium-triggered membrane interaction of the alpha-
770 synuclein acidic tail. *Biochemistry* **45,** 10947–10956 (2006).

771 32. Cárdenas, A. M. & Marengo, F. How the stimulus defines the dynamics of vesicle pool
772 recruitment, fusion mode and vesicle recycling in neuroendocrine cells. *J. Neurochem.*
773 n/a-n/a (2016).

774 33. Larsen, K. E. *et al.* Alpha-synuclein overexpression in PC12 and chromaffin cells
775 impairs catecholamine release by interfering with a late step in exocytosis. *J. Neurosci.*
776 **26,** 11915–11922 (2006).

777 34. Scott, D. A. *et al.* A Pathologic Cascade Leading to Synaptic Dysfunction in α-Synuclein-
778 Induced Neurodegeneration. *J. Neurosci.* **30,** 8083–8095 (2010).

779 35. Nemani, V. M. *et al.* Increased Expression of Alpha-Synuclein Reduces
780 Neurotransmitter Release by Inhibiting Synaptic Vesicle Reclustering After
781 Endocytosis. *Neuron* **65,** 66–79 (2010).
782 36. Wu, N., Joshi, P. R., Cepeda, C., Masliah, E. & Levine, M. S. Alpha-Synuclein
783 overexpression in mice alters synaptic communication in the corticostriatal pathway.
784 *J. Neurosci. Res.* **88,** 1764–1776 (2010).
785 37. Janezic, S. *et al.* Deficits in dopaminergic transmission precede neuron loss and
786 dysfunction in a new Parkinson model. *Proc. Natl. Acad. Sci.* **110,** E4016–E4025
787 (2013).
788 38. Yavich, L., Tanila, H., Vepsäläinen, S. & Jäkälä, P. Role of α-Synuclein in Presynaptic
789 Dopamine Recruitment. *J. Neurosci.* **24,** 11165–11170 (2004).
790 39. Senior, S. L. *et al.* Increased striatal dopamine release and hyperdopaminergic-like
791 behaviour in mice lacking both alpha-synuclein and gamma-synuclein. *Eur. J. Neurosci.*
792 **27,** 947–957 (2008).
793 40. Chandra, S. *et al.* Double-knockout mice for Effect on synaptic functions α- and β-
794 synucleins: *Proc. Natl. Acad. Sci. U. S. A.* **101,** 14966–71 (2004).
795 41. Anwar, S. *et al.* Functional alterations to the nigrostriatal system in mice lacking all
796 three members of the synuclein family. *J. Neurosci.* **31,** 7264–7274 (2011).
797 42. Burre, J. The Synaptic Function of a-Synuclein. *J Park. Dis.* **5,** 699–713 (2015).
798 43. Lautenschläger, J., Kaminski, C. F. & Kaminski Schierle, G. S. α-Synuclein – Regulator of
799 Exocytosis, Endocytosis, or Both? *Trends Cell Biol.* **27,** 468-479 (2017).
800 44. Diao, J. *et al.* Native α-synuclein induces clustering of synaptic-vesicle mimics via
801 binding to phospholipids and synaptobrevin-2/VAMP2. *Elife* **2,** e00592 (2013).
802 45. Scott David, R. S. Alpha-synuclein inhibits inter-synaptic vesicle mobility and maintains

803 recycling-pool homeostasis. *J. Neurosci.* **32,** 10129–10135 (2012).

804 46. Wang, L. *et al.* A-Synuclein Multimers Cluster Synaptic-Vesicles and Attenuate
805 Recycling. *Curr Biol.* **24,** 2319–2326 (2014).

806 47. Greten-Harrison, B. *et al.* αβγ-Synuclein triple knockout mice reveal age-dependent
807 neuronal dysfunction. *Proc. Natl. Acad. Sci. U. S. A.* **107,** 19573–8 (2010).

808 48. Clayton, D. F. & George, J. M. The synucleins: a family of proteins involved in synaptic
809 function, plasticity, neurodeneration and disease. *Tins* **21,** 249–254 (1998).

810 49. Leong, S. L. *et al.* Formation of dopamine-mediated α-synuclein-soluble oligomers
811 requires methionine oxidation. *Free Radic. Biol. Med.* **46,** 1328–1337 (2009).

812 50. German, D. C., Manaye, K. F., Sonsalla, P. K. & Brooks, B. a. Midbrain dopaminergic
813 cell loss in Parkinson's disease and MPTP-induced parkinsonism: sparing of calbindin-
814 D28k-containing cells. *Ann. N. Y. Acad. Sci.* **648,** 42–62 (1992).

815 51. Guzman, J. N., Sanchez-Padilla, J., Chan, C. S. & Surmeier, D. J. Robust Pacemaking in
816 Substantia Nigra Dopaminergic Neurons. *J Neurosci* **29,** 11011–19 (2009).

817 52. Galvagnion, C. *et al.* Lipid vesicles trigger α-synuclein aggregation by stimulating
818 primary nucleation. *Nat. Chem. Biol.* **11,** 229–234 (2015).

819 53. Masliah, E. *et al.* Passive immunization reduces behavioral and neuropathological
820 deficits in an alpha-synuclein transgenic model of lewy body disease. *PLoS One* **6,**
821 (2011).

822 54. Oertel, W. & Schulz, J. B. Current and experimental treatments of Parkinson disease: A
823 guide for neuroscientists. *J. Neurochem.* **139,** 325–337 (2016).

824 55. Schneider, S. A. *et al.* Can we use peripheral tissue biopsies to diagnose Parkinson's
825 disease? A review of the literature. *Eur. J. Neurol.* **23,** 247–261 (2016).

826 56. Huang, C., Ren, G., Zhou, H. & Wang, C. A new method for purification of recombinant

827 human alpha-synuclein in Escherichia coli. *Protein Expr. Purif.* **42,** 173–177 (2005).
828 57. Campioni, S. *et al.* The Presence of an Air−Water Interface Affects Formation and
829 Elongation of α‑Synuclein Fibrils. (2014). doi:10.1021/ja412105t
830 58. Ahmed, S., Holt, M., Riedel, D. & Jahn, R. Small-scale isolation of synaptic vesicles
831 from mammalian brain. *Nat. Protoc.* **8,** 998–1009 (2013).
832 59. Dunkley, P. R., Jarvie, P. E. & Robinson, P. J. PROTOCOL A rapid Percoll gradient
833 procedure for preparation of synaptosomes. **3,** (2008).
834 60. Ahmed, R. *et al.* Molecular mechanism for the (-)-Epigallocatechin gallate-induced
835 toxic to nontoxic remodeling of Aβ oligomers. *J. Am. Chem. Soc.* **139,** 13720–13734
836 (2017).
837 61. Algamal, M. *et al.* Atomic-resolution map of the interactions between an amyloid
838 inhibitor protein and amyloid β (Aβ) peptides in the monomer and protofibril states. *J.*
839 *Biol. Chem.* **292,** 17158–17168 (2017).
840 62. Huang, H., Milojevic, J. & Melacini, G. Analysis and optimization of saturation transfer
841 difference NMR experiments designed to map early self-association events in
842 amyloidogenic peptides. *J. Phys. Chem. B* **112,** 5795–5802 (2008).
843 63. Fawzi, N. L., Ying, J., Ghirlando, R., Torchia, D. A. & Clore, G. M. Atomic-resolution
844 dynamics on the surface of amyloid-β protofibrils probed by solution NMR. *Nature*
845 **480,** 268–272 (2011).
846 64. Vallurupalli, P., Bouvignies, G. & Kay, L. E. Studying 'invisible' excited protein states in
847 slow exchange with a major state conformation. *J. Am. Chem. Soc.* **134,** 8148–8161
848 (2012).
849 65. Milojevic, J., Esposito, V., Das, R. & Melacini, G. Understanding the Molecular Basis for
850 the Inhibition of the Alzheimer ' s A -Peptide Oligomerization by Human Serum

851 Albumin Using Saturation Transfer Difference and Off-Resonance Relaxation NMR
852 Spectroscopy. *Methods* 4282–4290 (2007).
853 66. Kuhn, P. *et al.* A facile protocol for the immobilisation of vesicles, virus particles,
854 bacteria, and yeast cells. *Integr. Biol. (Camb).* **4,** 1550–5 (2012).
855 67. Pinotsi, D. *et al.* Direct Observation of Heterogeneous Amyloid Fibril Growth Kinetics
856 via Two-Color Super-Resolution Microscopy. *Nano Lett.* **14,** 339–345 (2014).
857 68. van de Linde, S. *et al.* Direct stochastic optical reconstruction microscopy with
858 standard fluorescent probes. *Nat. Protoc.* **6,** 991–1009 (2011).
859 69. Tokunaga, M., Imamoto, N. & Sakata-Sogawa, K. Highly inclined thin illumination
860 enables clear single-molecule imaging in cells. *Nat. Methods* **5,** 159–61 (2008).
861 70. Wolter, S. *et al.* rapidSTORM : accurate , fast open-source software for localization
862 microscopy orcae : online resource for community annotation of eukaryotes. *Nat.*
863 *Methods* **9,** 1040–1 (2012).
864 71. Rees, E. J. *et al.* Elements of image processing in localization microscopy. *J. Opt.* **15,**
865 94012 (2013).
866 72. Schindelin, J. *et al.* Fiji: an open-source platform for biological-image analysis. *Nat.*
867 *Methods* **9,** 676–682 (2012).
868 73. Owen, D. M. *et al.* PALM imaging and cluster analysis of protein heterogeneity at the
869 cell surface. *J. Biophotonics* **3,** 446–454 (2010).
870 74. de Chaumont, F. *et al.* Icy: an open bioimage informatics platform for extended
871 reproducible research. *Nat. Methods* **9,** 690–696 (2012).
872 75. Olivo-Marin, J. C. Extraction of spots in biological images using multiscale products.
873 *Pattern Recognit.* **35,** 1989–1996 (2002).
874 76. Manders, E. M. M., Verbeek, F. J. & Aten, J. A. Measurement of co-localization of

875 objects in dualcolor confocal images. *J. Microsc.* **169,** 375–382 (1993).

876 77. Giehm, L. & Otzen, D. E. Strategies to increase the reproducibility of protein

877 fibrillization in plate reader assays. *Anal. Biochem.* **400,** 270–281 (2010).

878

879

880

881 **Author Contributions**

882 G.F. and A.DS. performed NMR studies. M.Z. and J.J.P. performed the mass spectrometry

883 studies. A.D.S. and N.N. performed the in vitro studies. A.D.S. and N.C. performed studies on

884 isolated synaptic vesicles. J.L., F.S., A.D.S. and A.T. contributed to synaptosome studies. J.L.,

885 F.S., C.H.M. and D.P. contributed to cell studies. J.L., A.D.S, F.S., E.R., M.F. and R.L. were

886 involved in data analysis. W.Z., A.T., P.F., P.StGH., C.F.K. and G.S.K. conceived and designed

887 the experiments. J.L., A.D.S., C.H.M and G.S.K conducted the overall manuscript.

888

889 **Acknowledgments**

890 We would like to thank Dr. Eugene Mosharov and Prof. David Sulzer for fruitful discussions.

891 J.L. was supported by a research fellowship from the Deutsche Forschungsgemeinschaft

892 (DFG; award LA 3609/2-1). M.Z. acknowledges funding from the Eugenides Foundation.

893 C.F.K. acknowledges funding from the UK Engineering and Physical Sciences Research

894 Council (EPSRC). A.DS. acknowledges funding from the UK Medical Research Council

895 (MRC, MR/N000676/1). A.DS. and G.F. acknowledge funding from Parkinson's UK (G-1508).

896 G.S.K. and C.F.K. acknowledge funding from the Wellcome Trust, the UK Medical Research

897 Council (MRC), Alzheimer Research UK (ARUK), and Infinitus China Ltd. J.L. and A.D.S.

898 acknowledge Alzheimer Research UK (ARUK) travel grants.

899

900 **Competing Financial Interest**

901 The authors declare no competing financial interests.

902

903

904

905 **Figure Legends**

906 **Figure 1. Calcium binding to the C-terminus of alpha-synuclein and lipid binding**

907 (A) ^{1}H-^{15}N HSQC NMR spectrum of alpha-synuclein in the absence (red) and in the presence
908 of calcium (green, 1.6 mM calcium). Major chemical shift perturbations in the presence of
909 calcium are located at the C-terminus of alpha-synuclein (red arrows with assigned amino
910 acid residues), while peak broadening (blue arrows with assigned amino acid residues) can
911 be seen within the NAC-region.

912 (B) Fitting of alpha-synuclein calcium binding (K_D) from ^{1}H-^{15}N HSQC NMR spectra at
913 increasing calcium concentrations, where L indicates the number of Ca^{2+} ions interacting
914 with one alpha-synuclein molecule.

915 (C) Calcium-bound alpha-synuclein species directly observed by mass spectrometry.
916 Electrospray ionisation mass spectra were acquired under identical instrument conditions
917 for samples incubated with or without calcium. Multiple alpha-synuclein species were
918 observed upon charge deconvolution of the ion envelope for the 9^{+} - 19^{+} charge states,
919 inclusive. The masses correspond to alpha-synuclein: calcium complexes up to a
920 stoichiometry of 1:6.

921 (D) Lipid pull down experiment using lipids from Folch brain extracts, recombinant alpha-
922 synuclein and various ions. Western blot of the amount of protein pulled down shows that

923 more alpha-synuclein was pulled down by the lipids in the presence of calcium. Neither
924 potassium, sodium, nor magnesium increased alpha-synuclein lipid binding to the same
925 extent. **p = 0.0011, 0.0022 and 0.0090 for comparison of 1 mM $CaCl_2$ with a-syn control,
926 50 mM KCl, and 150 mM NaCl, respectively. Calculated using one-way ANOVA with Tukey's
927 post hoc correction, graphs indicate mean +/- s.e.m.. N = 3 for all groups, corresponding to 3
928 biological repeats, d.f. 12.
929
930 **Figure 2. The C-terminus of alpha-synuclein binds to synaptic vesicles upon calcium binding**
931 (A) CEST NMR experiments were performed on alpha-synuclein and synaptic vesicles in the
932 absence (black) or presence of calcium (red, 6 mM). In the absence of calcium, the N-
933 terminus shows the strongest interaction with synaptic vesicles. Upon addition of calcium,
934 the interaction of the C-terminus and also of some residues of the NAC-region increases,
935 which is seen as a reduction of the signal. Experiments were repeated twice.
936 (B) Lipid pull down experiment showing the transient nature of alpha-synuclein lipid binding.
937 Western blot of the amount of alpha-synuclein pulled down by the lipids showing that
938 calcium-induced lipid binding of alpha-synuclein is reversible upon addition of the calcium
939 chelator EGTA. *p = 0.0263, calculated using one-way ANOVA with Tukey's post hoc
940 correction, graphs indicate mean +/- s.e.m.. N = 6 for control and $CaCl_2$, n = 4 for EGTA and
941 $CaCl_2$ + EGTA, data from 3 biological repeats, d.f. 16.
942 (C) *d*STORM super-resolution imaging of alpha-synuclein and VAMP2 on isolated
943 synaptosomes displaying alpha-synuclein clustering under normal physiological conditions
944 with 2.5 mM calcium in the extracellular buffer (upper panel). Upon calcium depletion in the
945 extracellular buffer, using 1 mM EGTA, alpha-synuclein localization was dispersed (lower
946 panel).

947 (D) Cluster analysis of alpha-synuclein and VAMP2 immunostaining showing increased
948 cluster size of alpha-synuclein upon calcium depletion, while VAMP2 cluster size is the same
949 either in the presence of calcium or upon calcium depletion in the extracellular buffer.
950 ****$p < 0.0001$, $^{ns}p = 0.6363$ calculated using two-tailed t-test, graphs indicate mean +/-
951 s.e.m.. N = 22 for + Ca^{2+} and n = 30 for - Ca^{2+}, where n indicates single synaptosomes, data
952 form 3 biological repeats, d.f. 50.
953
954 **Figure 3. Alpha-synuclein and calcium balance the interaction of synaptic vesicles**
955 (A) STED super-resolution imaging of isolated synaptic vesicles incubated with 1 mM EGTA,
956 200 µM calcium, 50 µM alpha-synuclein + 200 µM calcium, or 50 µM alpha-synuclein + 1 mM
957 EGTA. Images show synaptic vesicles circled in red as detected for analysis of synaptic vesicle
958 clustering. Scales represent 200 nm. Synaptic vesicle clustering is shown as a decrease of
959 synaptic vesicles found as single vesicles and as an increase of synaptic vesicles found in
960 clusters was seen upon incubation of synaptic vesicles with either increased calcium or
961 alpha-synuclein. Note, EGTA was not able to reduce synaptic vesicle clustering in the
962 presence of increased alpha-synuclein concentrations. **$p = 0.0023$, ****$p < 0.0001$ and **p
963 $= 0.0012$ for comparison of % of single vesicles, *$p = 0.0140$, ***$p = 0.0001$ and *$p = 0.0136$
964 for comparison of % of vesicle clusters of two. Calculated using two-way ANOVA with
965 Tukey's post hoc correction, graphs indicate mean +/- s.e.m.. N = 18 for all conditions, data
966 from biological 3 repeats, d.f. 272.
967 (B) TEM images of synaptic vesicles showing synaptic vesicle clustering in the presence of 50
968 µM alpha-synuclein.

969 (C) Combined imaging of synaptic vesicles (confocal) and ATTO647N labelled alpha-synuclein
970 (STED) showing synaptic vesicles surrounded and glued together by alpha-synuclein. 2
971 biological repeats.
972
973 **Figure 4. Calcium and alpha-synuclein levels mediate dopamine toxicity**
974 (A-C) Ventral midbrain neurons were incubated with 100 µM dopamine in the presence or
975 absence of 5 µM isradipine. *d*STORM super-resolution microscopy of alpha-synuclein and
976 synaptotagmin 1 after 72 h revealed an increase in the area of alpha-synuclein puncta, an
977 increase in the size of synaptotagmin 1 puncta and an increased colocalization of alpha-
978 synuclein with synaptotagmin 1 upon dopamine treatment. These effects were reversed by
979 the $Ca_v1.3$ calcium channel antagonist isradipine, showing decreased size of alpha-synuclein
980 and synaptotagmin-1 puncta and decreased colocalization. ****$p < 0.0001$ for
981 synaptotagmin and alpha-synuclein, **$p < 0.0066$, *$p < 0.0446$ for colocalization, calculated
982 using one-way ANOVA with Tukey's post hoc correction, graphs indicate mean +/- s.e.m.. N =
983 2251, 1154, 1987 for synaptotagmin, d.f. 5353, n = 5198, 3210, 6845 for alpha-synuclein, d.f.
984 15250, where n indicates individual clusters identified from 30, 30, 29 images from 3
985 biological repeats, n= 30, 30, 29 for colocalization, where n indicates number of images.
986 (D) Dopamine toxicity in SH-SY5Y cells after 72 h incubation with 100 µM dopamine was
987 rescued upon treatment with 5 µM isradipine and upon alpha-synuclein knock-down,
988 showing that both, calcium and alpha-synuclein are necessary for toxicity to occur. ***$p <$
989 0.0007, $^{ns}p = 0.9935$ for isradipine, n = 12 for all groups, where n indicates number of wells,
990 d.f. 44; **$p < 0.0062$, $^{ns}p = 0.9934$ for alpha-synuclein knock-out, n = 8 for all groups, where
991 n indicates wells, d.f. 28, calculated using one-way ANOVA with Tukey's post hoc correction,
992 graphs indicate mean +/- s.e.m.. 3 biological repeats.

993

994 **Figure 5. The effect of calcium and synaptic vesicles on alpha-synuclein aggregation**

995 (A) Alpha-synuclein aggregation measured by ThT fluorescence using 100 µM monomeric
996 alpha-synuclein under shaking conditions. The presence of 2.5 mM calcium increased the
997 aggregation kinetics of alpha-synuclein compared to 1 mM EGTA, both in the presence or
998 absence of synaptic vesicles (black and red). For the EGTA-containing groups there was a
999 trend towards faster aggregation of alpha synuclein in the presence of synaptic vesicles (blue
1000 vs. grey). 3 biological repeats, n = 18 for all conditions, where n represents single wells.
1001 values represent mean +/- s.e.m..

1002 (B) TEM images of alpha-synuclein fibrils formed in the presence of 2.5 mM calcium or 1
1003 mM EGTA either in the presence or absence of synaptic vesicles. Differences in the
1004 morphology of alpha-synuclein fibrils were observed for fibrils formed in the presence of 2.5
1005 mM calcium in the absence and presence of synaptic vesicles. In the presence of synaptic
1006 vesicles alpha-synuclein fibrils showed increased lateral bundling and shortening. Alpha-
1007 synuclein aggregation in the presence of 1 mM EGTA led to substantially less fibrils, however
1008 the fibrils formed, retained their morphological phenotype compared to the fibrils formed in
1009 the presence of 2.5 mM calcium. Alpha-synuclein fibrils formed in the presence of synaptic
1010 vesicles plus 1 mM EGTA showed an intermediate phenotype, with bundled, but more
1011 elongated fibril structures than found in the synaptic vesicles and 2.5 mM calcium group.
1012 Experiments were repeated twice.

1013

1014 **Table 1. The effect of calcium and synaptic vesicles on alpha-synuclein aggregation**

1015

Condition	lag time (hours)	k_1 (ms^{-1})	k_2 (s^{-1} $\%int^{-1}$)	remaining monomer (µM)

Ca^{2+} only	3.95 ± 0.53	0.24 ± 0.69	8.07 ± 1.28	8.5 ± 0.3 ****
Ca^{2+} + SV	5.55 ± 2.59	0.78 ± 5.33	15.92 ± 5.02	_[a]
EGTA only	78.95 ± 0.42	0.09 ± 0.04	6.32 ± 0.65	67.8 ± 5.4
EGTA + SV	44.72 ± 0.42	0.22 ± 0.06	5.50 ± 0.51	_[a]

1016

1017 ThT fluorescence intensity profiles were used to calculate the lag time as well as the
1018 nucleation (k_1) and the elongation rate (k_2). Lag time is given as X intercept with standard
1019 error. k_1 and k_2 are given as constants with a 95 % confidence interval. 3 biological repeats.
1020 Remaining alpha-synuclein monomer concentration was revealed by analytical SEC-HPLC at
1021 the end of the experiment. ****$p < 0.0001$, n = 10 for Ca^{2+} only and n = 9 for EGTA only,
1022 where n indicates wells, 2 biological repeats, calculated using two-tailed t-test, values
1023 indicate mean +/- s.e.m.. d.f. 17. [a] Remaining monomer concentration could not be
1024 calculated due to presence of protein from synaptic vesicles preventing clear detection of
1025 remaining asyn monomer.
1026

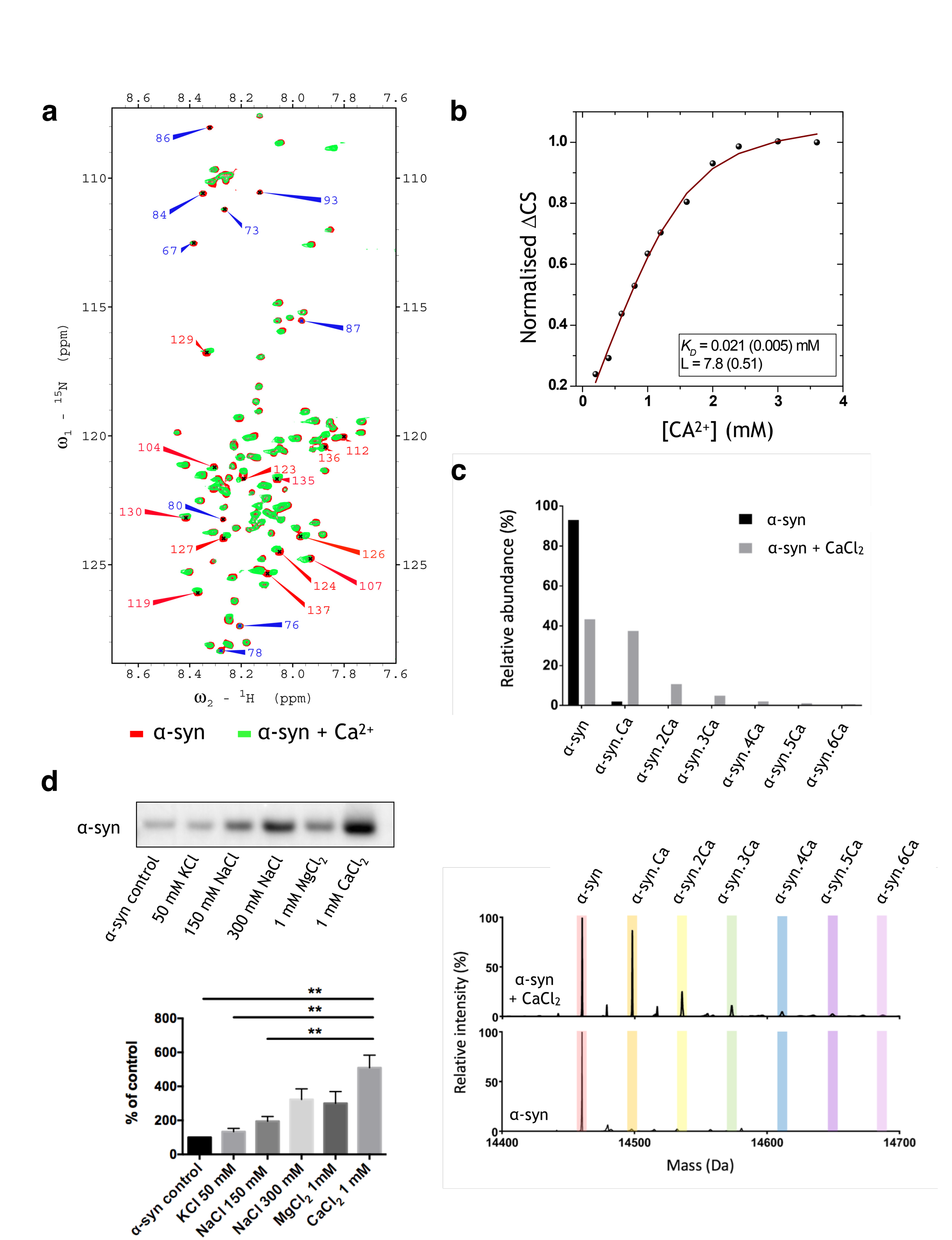
a
8.6 8.4 8.2 8.0 7.8 7.6
110
115
120
125
ω_1 - ^{15}N (ppm)
ω_2 - ^{1}H (ppm)
86
84
93
73
67
87
129
104
112
136
123
135
130
80
127
126
124
107
119
137
76
78
α-syn
α-syn + Ca2+
b
Normalised ΔCS
[CA2+] (mM)
K_D = 0.021 (0.005) mM
L = 7.8 (0.51)
c
Relative abundance (%)
α-syn
α-syn + CaCl2
α-syn
α-syn.Ca
α-syn.2Ca
α-syn.3Ca
α-syn.4Ca
α-syn.5Ca
α-syn.6Ca
d
α-syn
α-syn control
50 mM KCl
150 mM NaCl
300 mM NaCl
1 mM MgCl2
1 mM CaCl2
% of control
α-syn control
KCl 50 mM
NaCl 150 mM
NaCl 300 mM
MgCl2 1mM
CaCl2 1 mM
Relative intensity (%)
α-syn + CaCl2
α-syn
Mass (Da)

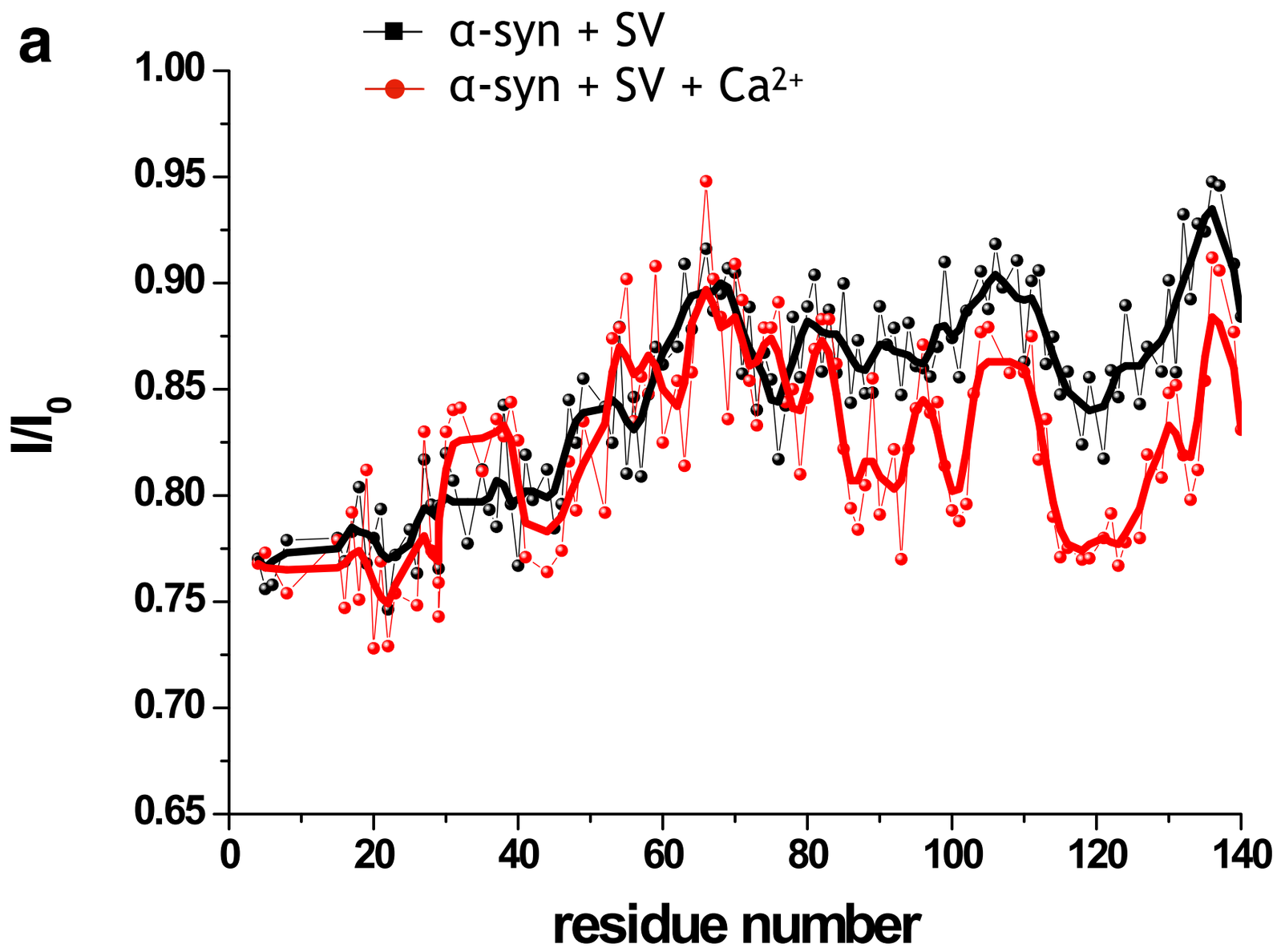
a
α-syn + SV
α-syn + SV + Ca2+
I/I0
1.00
0.95
0.90
0.85
0.80
0.75
0.70
0.65
0
20
40
60
80
100
120
140
residue number

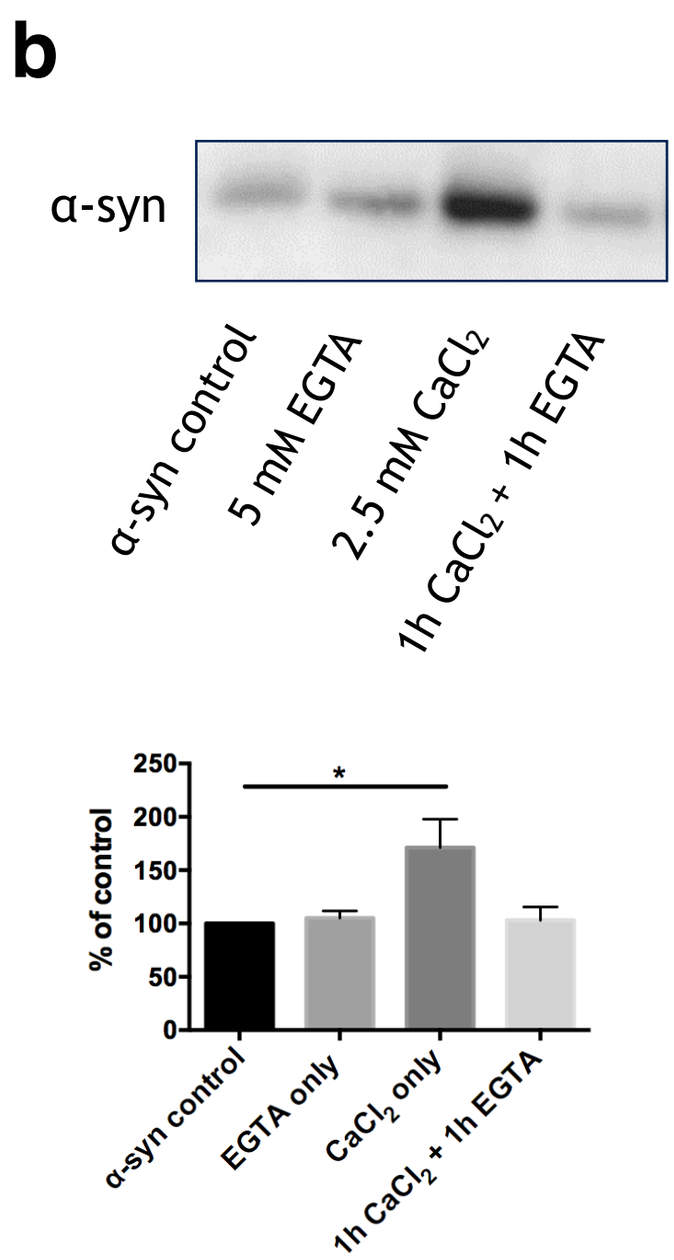
b
α-syn
α-syn control
5 mM EGTA
2.5 mM CaCl2
1h CaCl2 + 1h EGTA
% of control
250
200
150
100
50
0
*
α-syn control
EGTA only
CaCl2 only
1h CaCl2 + 1h EGTA

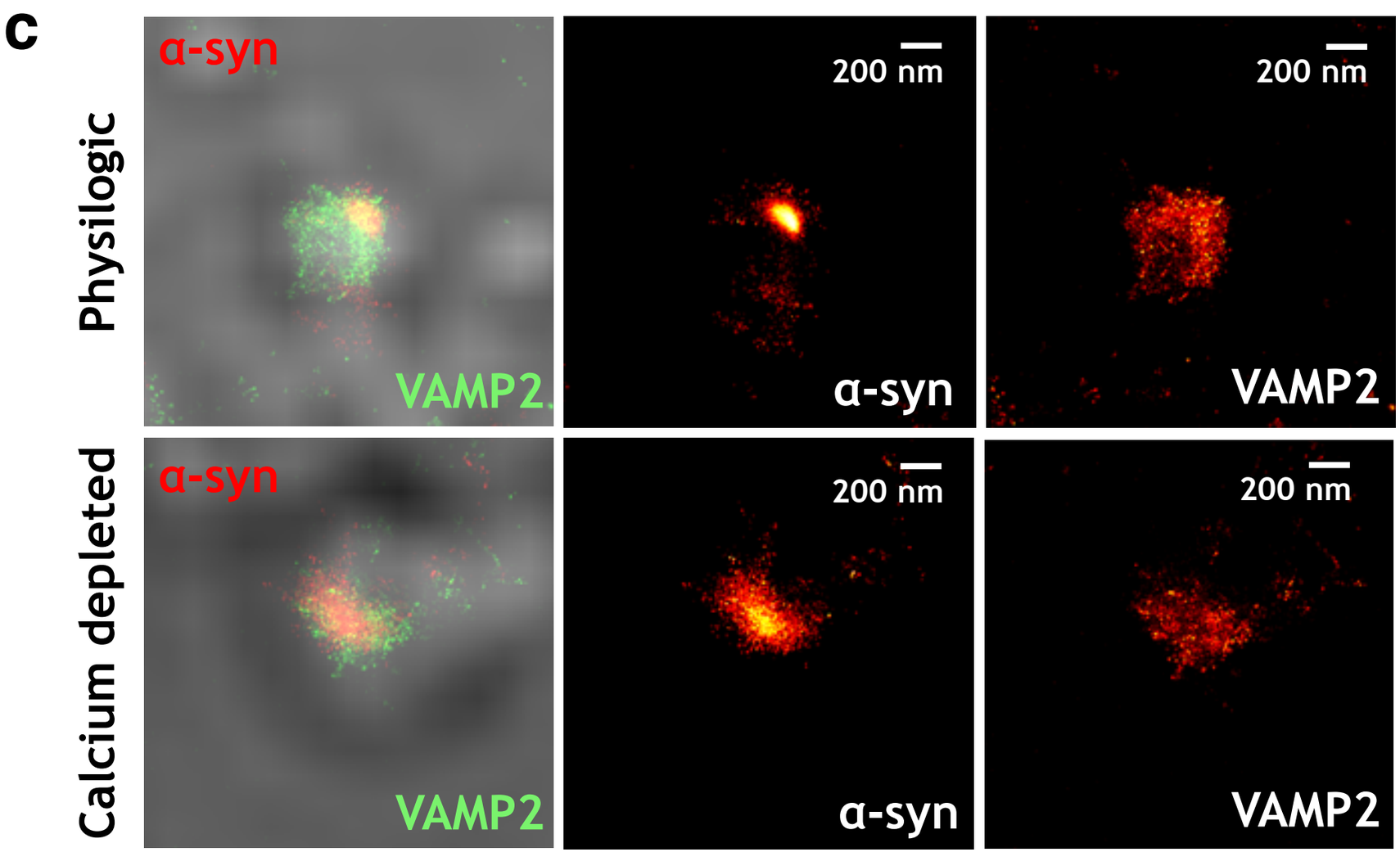
c
Physilogic
Calcium depleted
α-syn
VAMP2
200 nm
α-syn
VAMP2

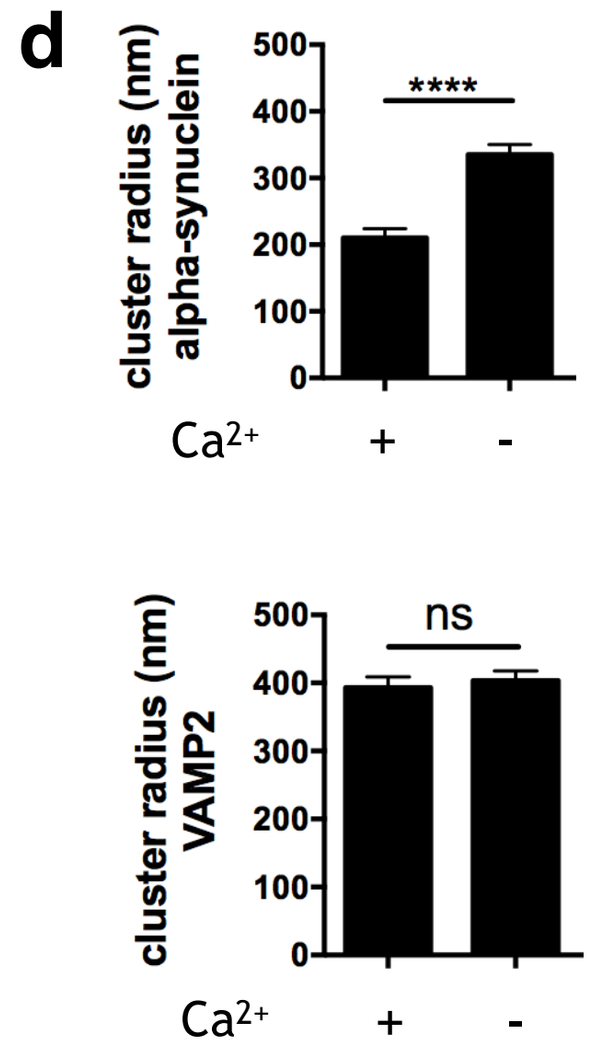
d
cluster radius (nm)
alpha-synuclein
500
400
300
200
100
0
****
Ca2+
+
-
cluster radius (nm)
VAMP2
ns

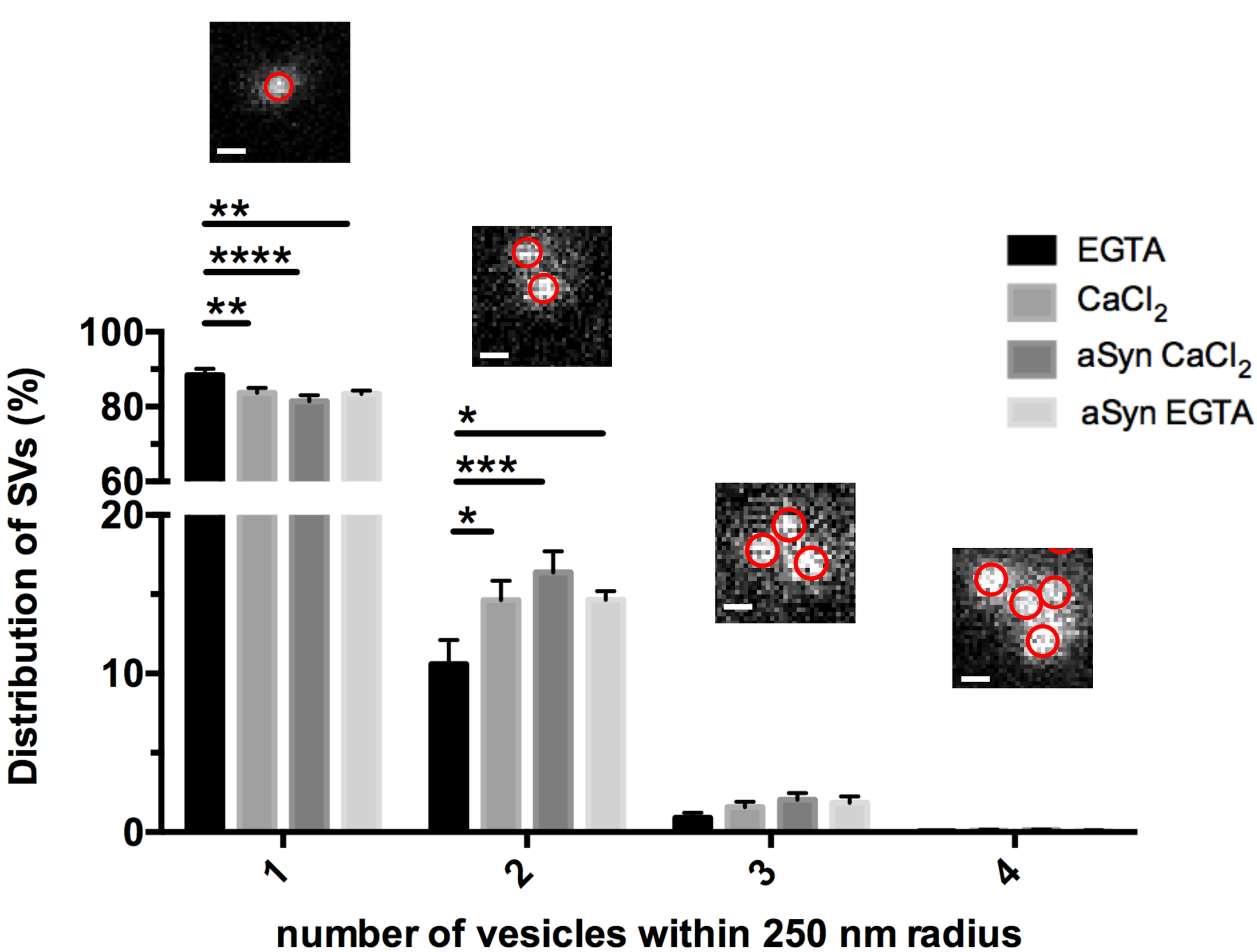
a
EGTA
CaCl2
aSyn CaCl2
aSyn EGTA
Distribution of SVs (%)
100
80
60
20
10
0
**
****
**
*
***
*
1
2
3
4
number of vesicles within 250 nm radius

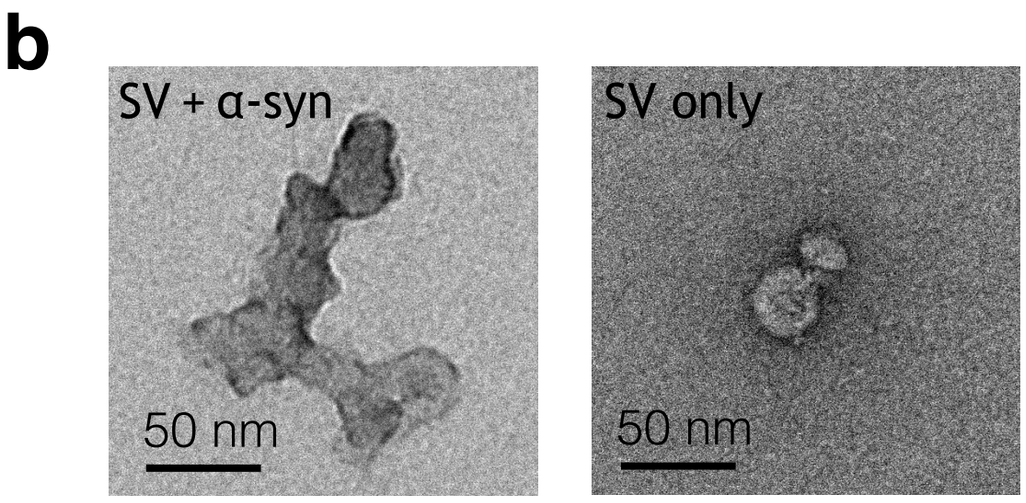
b
SV + α-syn
50 nm
SV only
50 nm

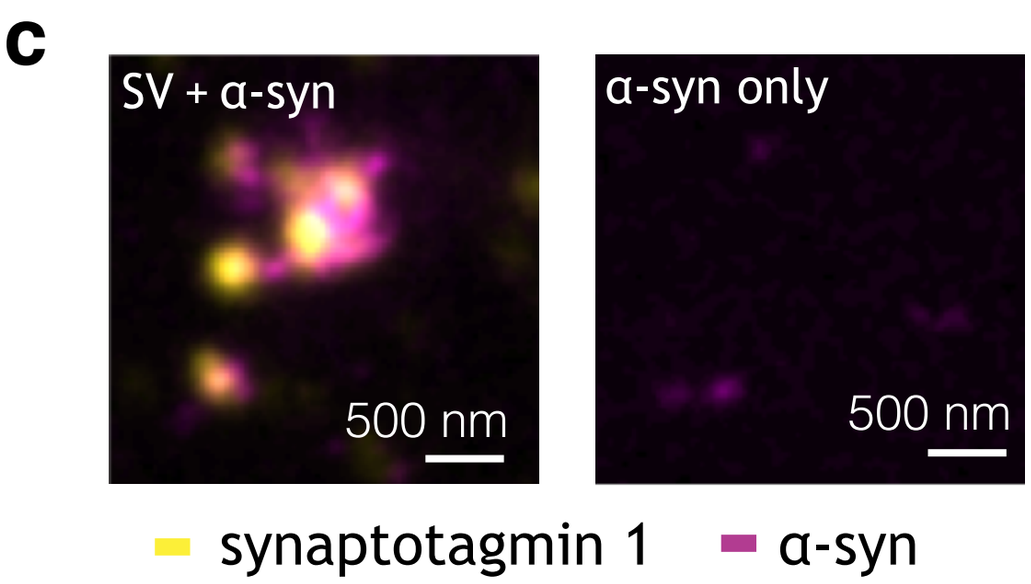
c
SV + α-syn
500 nm
α-syn only
500 nm
synaptotagmin 1
α-syn

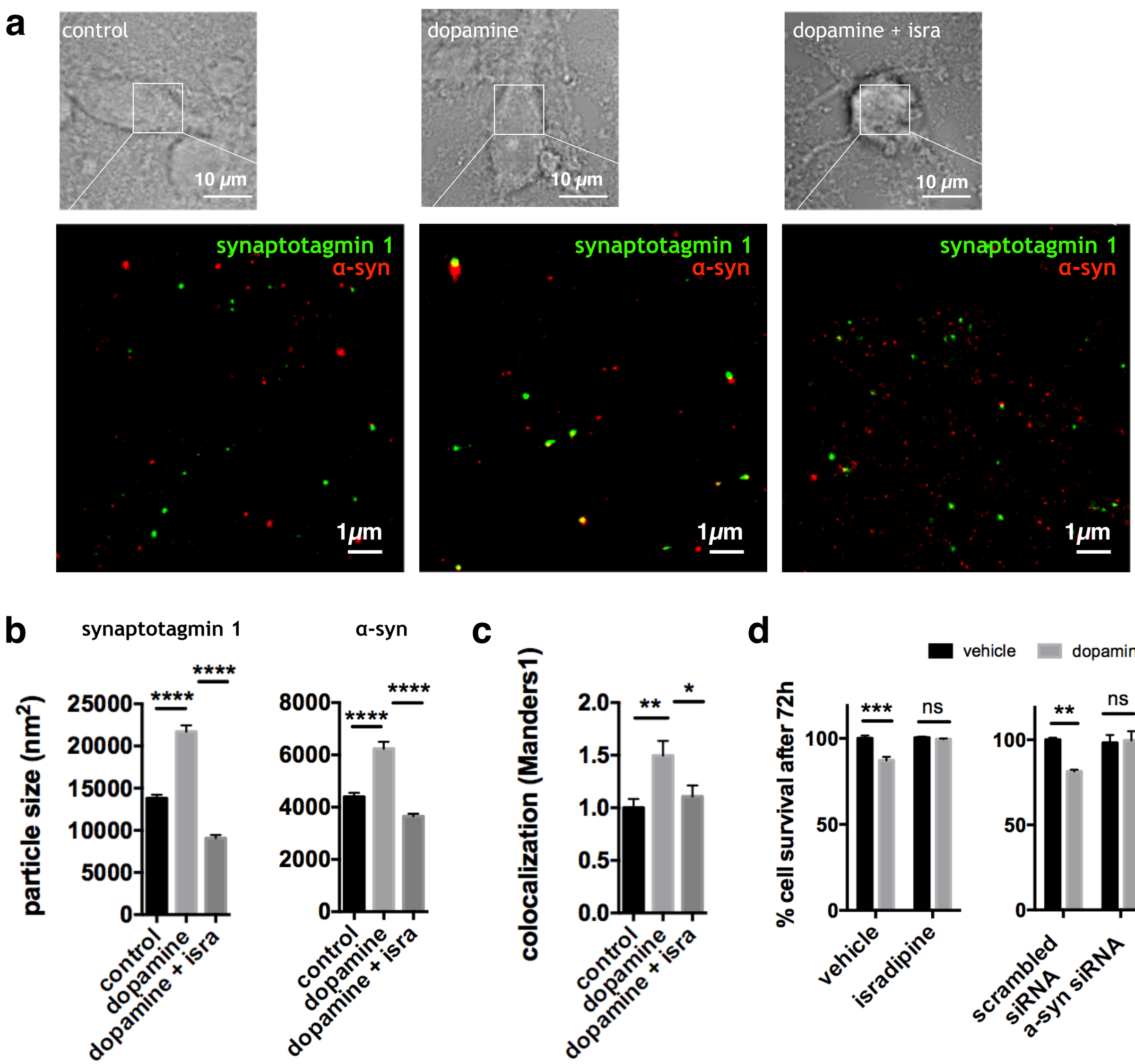
a
control
dopamine
dopamine + isra
10 μm
synaptotagmin 1
α-syn
1μm
b
synaptotagmin 1
α-syn
particle size (nm²)
25000
20000
15000
10000
5000
0
8000
6000
4000
2000
****
control
dopamine
dopamine + isra
c
colocalization (Manders1)
2.0
1.5
1.0
0.5
0.0
**
*
d
vehicle
dopamine
% cell survival after 72h
100
50
0
***
ns
**
vehicle
isradipine
scrambled siRNA
a-syn siRNA

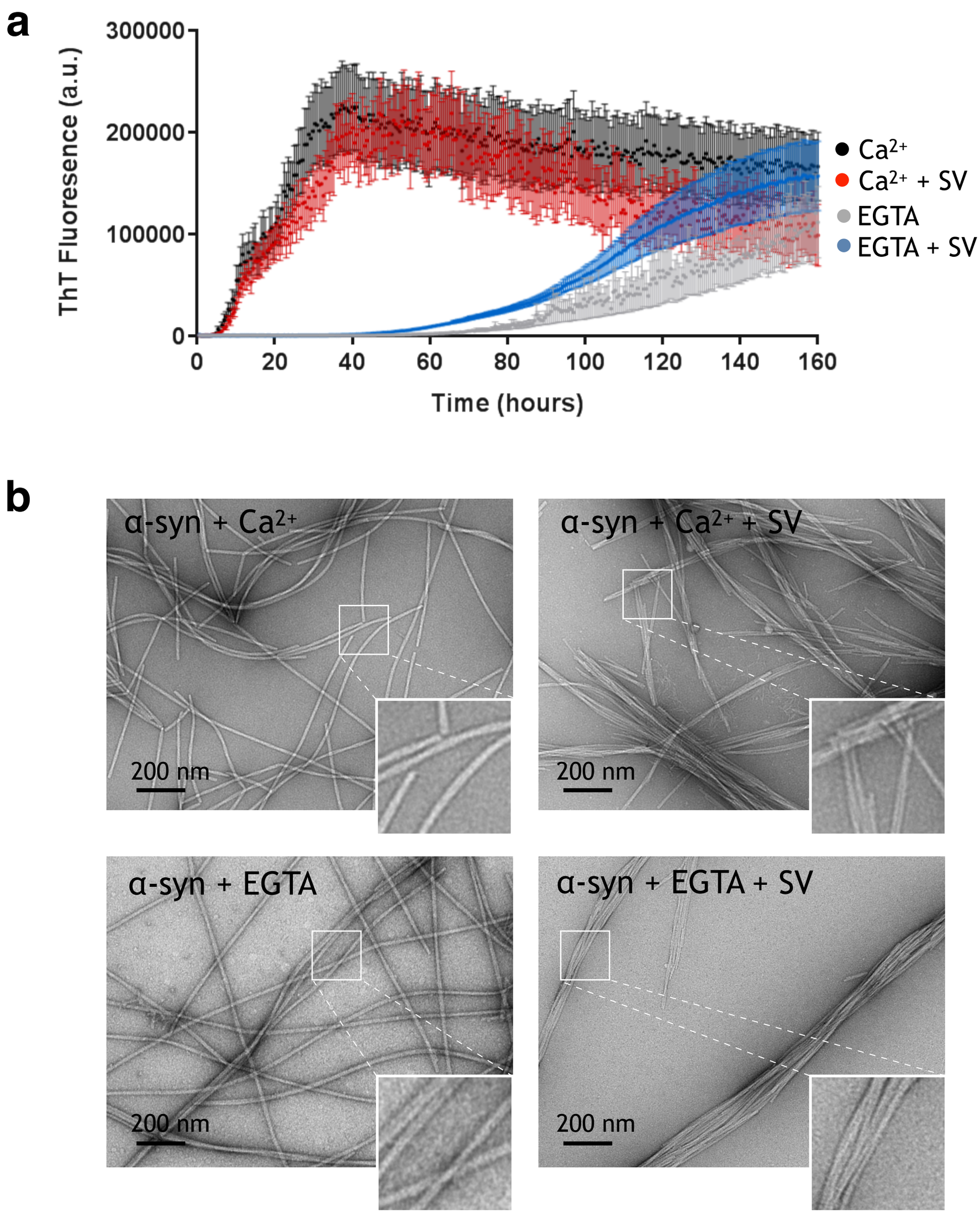
a
300000
200000
100000
0
ThT Fluoresence (a.u.)
0
20
40
60
80
100
120
140
160
Time (hours)
Ca2+
Ca2+ + SV
EGTA
EGTA + SV
b
α-syn + Ca2+
200 nm
α-syn + Ca2+ + SV
200 nm
α-syn + EGTA
200 nm
α-syn + EGTA + SV
200 nm